

PREVENTION OF MUSCULAR DYSTROPHY IN MICE BY GENE EDITING

APPROVED BY SUPERVISORY COMMITTEE

Eric N. Olson, Ph.D.

Melanie H. Cobb, Ph.D.

Zhijian Chen, Ph.D.

Zhigao Wang, Ph.D.

DEDICATION

In dedication to my mother Daoying YANG for giving me everything.

Acknowledgements

Five years ago, when I boarded the plane to Dallas in Beijing on a warm day, I certainly didn't know what my life was going to be in the next few years. It turned out to be a fantastic adventure, full of smiles, sweat and tears. I am really grateful for all the encouragement and support from the great people around me.

My sincere appreciation goes to my mentor Dr. Eric Olson. He reshaped my way of thinking on how to do research. I joined the lab in 2010, when I knew little about molecular biology and genetics. As soon as I joined the lab, I was really impressed by his never-ending passion about science. As a great leader of a huge lab and the department, he discussed the experiments and projects with me and offered suggestions almost every week over the past few years. He is a well-established scientist in the field, however, he never hesitated to explore new ground. Just one year ago, in the last year of my graduate studies, we thought that the new gene editing technology holds a great potential to cure human genetic diseases. Despite the fact that I knew little about the new technology or the disease, he enthusiastically supported this idea and shared his brilliant insights on the project shown in this thesis.

I am also really grateful to Dr. Rhonda Bassel-Duby for all her help in the past few years. I thank her for devoting her valuable time on teaching me both mouse genetics and academic skills, such as presentation and writing. She also taught me how to communicate with different collaborators. Research is not an easy job in any aspect, however, she always encouraged and supported me when I faced these challenges. I honestly appreciate her and her husband Dr. Allan D. Duby for taking care of me when I had medical issues last year.

I would like to thank my thesis committee members, Drs. Melanie Cobb, James Zhijian Chen and Zhigao Wang for their support. Melanie always gave me warm encouragement and insightful suggestions whenever we discussed my projects. James was also generous to share instruments in his lab. Zhigao introduced the CRISPR/Cas9 system to me and kept his door open whenever I had questions.

Obviously, without great team members I cannot even imagine finishing all the work within such a short time period. John R. McAnally, who is an expert on the mouse embryo manipulation and gene editing, conquered all the technical difficulties. John M. Shelton, a great histologist and molecular pathologist offered his insights and criticisms. His elegant work helped us obtain more detailed information about our project. Alex A. Mireault, who is a young talented researcher, finished all the experiments better than we had expected. All the team members maintained their enthusiasm and positive energy and stayed humble, friendly and happy all the time.

I thank Benjamin Nelson, Douglas Anderson and Kelly Anderson for advice and constructive criticism on the project. I thank Lillian Sutherland, Leonela Amoasii, Huanyu Zhou and Junyao Ren for discussions and technical help. I am grateful for suggestions and help from Dr. Robert Hammer and John Ritter in the Transgenic Core Facility, and Dr. James Richardson in the Molecular Pathology Core Facility at UTSW. I appreciate Jose Cabrera's work with graphics.

In addition, I would like to thank all the former and current members in the Olson lab, who created and maintained a unique environment for the great science, especially the postdocs who worked with me on different projects: Drs. Kunhua Song and Chad Grueter on the CAMTA1

project, Dr. Mayssa Mokalled on the MASTR project and Dr. Ning Liu on the novel myokine projects.

I would like to thank my family, especially my mother Daoying Yang and father Zhenji Long. Confucius remarked “While his parents are living, a son should not go far abroad”. However, they supported me to pursue my dream with their unconditional love, which I will never be able to completely pay back. Wenchan Zhao, my wife, who joined me in Dallas two years ago, is a great partner in both life and work. I am grateful to have such a wonderful family.

Again, it might be the time to say goodbye to the city of Dallas, though I still wonder what my life is going to be in the next few years. I am quite certain that it is going to be another wonderful journey.

PREVENTION OF MUSCULAR DYSTROPHY IN MICE BY GENE EDITING

by

CHENGZU LONG

DISSERTATION

Presented to the Faculty of the Graduate School of Biomedical Sciences

The University of Texas Southwestern Medical Center

In Partial Fulfillment of the Requirements

For the Degree of

DOCTOR OF PHILOSOPHY

The University of Texas Southwestern Medical Center

Dallas, Texas

December, 2014

Copyright

by

CHENGZU LONG 2014

All Rights Reserved

PREVENTION OF MUSCULAR DYSTROPHY IN MICE BY GENE EDITING

CHENGZU LONG, M.S.

The University of Texas Southwestern Medical Center, 2014

ERIC N. OLSON, Ph.D.

Duchenne muscular dystrophy (DMD) is an inherited X-linked disease caused by mutations in the gene encoding dystrophin, a protein required for muscle fiber integrity. DMD is characterized by progressive muscle weakness and a shortened lifespan, often along with breathing and heart complications. There is no effective treatment.

RNA-guided nucleases-mediated genome editing, based on Type II CRISPR/Cas systems, offers a new approach to alter the genome. It can precisely remove a mutation in DNA, allowing the DNA repair mechanisms to replace it with a normal copy of the gene. The benefit of this over other gene therapy techniques is that it can permanently correct the ‘defect’ in a gene rather than just transiently adding a ‘functional’ one.

We used CRISPR/Cas9-mediated genome editing to correct the dystrophin gene (*Dmd*) mutation in the germline of *mdx* mice, a model for DMD, and then monitored skeletal muscle and heart structure and function. Genome editing produced genetically mosaic animals

containing 2 to 100% correction of the *Dmd* gene. Histological analysis of skeletal muscle and heart from these corrected mice showed absence of the dystrophic muscle phenotype and restoration of dystrophin expression. In addition, the degree of muscle phenotypic rescue in mosaic mice exceeded the efficiency of gene correction, likely reflecting an advantage of the corrected stem cells and their contribution to regenerating muscle.

Our experiments provide proof-of-concept that CRISPR/Cas9-mediated genomic editing can correct a causative germline mutation causing muscular dystrophy in a mouse model and prevent development of several characteristic features of the disease. With rapid technological advances of gene delivery systems and improvements to the CRISPR/Cas9 editing system, this strategy may allow correction of disease-causing mutations in the muscle tissue or iPSCs (induced pluripotent stem cells) from patients with genetic diseases.

Table of Contents

Title.....	i
Dedication.....	ii
Acknowledgements.....	iii
Abstract.....	viii
Table of Contents.....	x
Publications.....	xiii
List of Figures.....	xiv
List of Tables.....	xvi
List of Abbreviations.....	xvii
Chapter 1 General Introduction.....	1
1.1 Introduction of DMD and dystrophin.....	2
1.2 Introduction of gene- or cell-based therapies.....	4
1.3 Introduction of CRISPR/Cas9 system.....	4
Chapter 2 CRISPR/Cas9-mediated gene editing in mice.....	7
2.1 Introduction.....	8
2.2 Design and synthesis of Cas9, gRNA and HDR templates.....	11
2.3 Optimization of the single blastocyst assay.....	12

2.4 CRISPR/Cas9-mediated gene editing in mice.....	14
2.5 Materials and Methods.....	19
Chapter 3 CRISPR/Cas9-mediated gene correction in <i>mdx</i> mice.....	25
3.1 Introduction.....	26
3.2 Design and synthesis of Cas9, gRNA- <i>mdx</i> and HDR template.....	27
3.3 CRISPR/Cas9-mediated gene correction.....	30
3.4 Genotyping of corrected <i>mdx</i> progeny.....	31
3.5 Sequencing of <i>mdx</i> -C.....	32
3.6 Materials and Methods.....	34
Chapter 4 Analysis of off-target effects	35
4.1 Introduction.....	36
4.2 Prediction of off-target sites.....	37
4.3 Deep sequencing.....	37
4.4 Materials and Methods.....	38
Chapter 5 Histological and functional analysis.....	45
5.1 Introduction.....	46
5.2 Immunohistochemical analysis.....	47
5.3 Western blot analysis.....	48
5.4 Functional assay.....	57

5.5 Materials and Methods.....	58
Chapter 6 A model for rescue of muscular dystrophy by CRISPR/Cas9.....	61
6.1 Introduction.....	62
6.2 Age-dependent improvement in <i>mdx-C</i> mice skeletal muscle.....	63
6.3 Analysis of satellite cells from <i>mdx-C</i> mice.....	67
6.4 Model to rescue DMD by genomic editing.....	70
6.5 Materials and Methods.....	71
Chapter 7 Discussion and future directions.....	74
Bibliography	77

Publications

1. **Long, C. ***, McAnally, JR.*, Shelton, JM., Mireault, AA., Bassel-Duby, R., Olson, EN. (2014) Prevention of muscular dystrophy in mice by CRISPR/Cas9-mediated editing of germline DNA. *Science* 345(6201):1184-8 (*These authors contributed equally).
2. **Long, C.***, Grueter, CE.*, Song, K.*, Qin, S., Qi, X., Kong, YM., Shelton, JM., Richardson, JA., Zhang, CL., Bassel-Duby, R., Olson, EN. (2014) Ataxia and Purkinje cell degeneration in mice lacking the CAMTA1 transcription factor. *Proceedings of the National Academy of Sciences of USA* 111(31):11521-6 (*These authors contributed equally).
3. Garg, A., O'Rourke, J., **Long, C.**, Doering, J., Ravenscroft, G., Bezprozvannaya, S., Nelson, BR., Beetz, N., Li, L., Chen, S., Laing, NG., Grange, RW., Bassel-Duby, R., Olson, EN. (2014) KLHL40 deficiency destabilizes thin filament proteins and promotes nemaline myopathy. *Journal of Clinical Investigation* 124(8):3529-39.

List of Figures

	Page
Figure 1.1 Schematic of the exons of human DMD and protein domains of dystrophin	3
Figure 1.2 Schematic outline of CRISPR/Cas9-mediated genomic targeting	5
Figure 1.3 Nuclease-induced genome editing	6
Figure 2.1 Design of guide RNA and HDR template	10
Figure 2.2 Design and synthesis of Cas9 mRNA and guide RNA	12
Figure 2.3 A single mouse blastocyst assay for detection of CRISPR/Cas9	13
Figure 2.4 Schematic of the PCR-based genotyping	15
Figure 2.5 PCR-based genotyping in edited mice	16
Figure 2.6 Sequencing results of PCR products from positive progeny mice	17
Figure 3.1 The molecular structure of dystrophin isoforms and the position of mutations in <i>mdx</i> mouse strains	27
Figure 3.2 Strategy of the gene correction in <i>mdx</i> mice via germ line gene therapy	28
Figure 3.3 CRISPR/Cas9-mediated <i>Dmd</i> correction in <i>mdx</i> mice	29
Figure 3.4 Strategy of the gene correction via HDR or NHEJ	30
Figure 3.5 Genotyping results of <i>mdx-C</i> mice	31
Figure 3.6 Direct sequencing results of WT, <i>mdx</i> and corrected <i>mdx-C</i> mice	32
Figure 3.7 Sequence of <i>Dmd</i> alleles present in F0 <i>mdx-C</i> mice	33
Figure 4.1. Deep sequencing analysis of target site and 32 theoretical off-target sites	39
Figure 5.1 Histological analysis of muscles from wild-type, <i>mdx</i> and <i>mdx-C</i> mice	49
Figure 5.2 Western blot analysis of heart and skeletal muscle samples	50
Figure 5.3. RFLP analysis and myofiber measurements of muscle	51
Figure 5.4 H&E and immunostaining of muscles from 7-9 week old wild-type, <i>mdx</i> , and <i>mdx-C</i> mice	53

Figure 5.5. Histology of muscles showing decrease in fibrosis and necrosis in 7-9 wks <i>mdx-C</i> mice	55
Figure 6.1 Satellite cell-mediated skeletal muscle regeneration	63
Figure 6.2 Progressive recovery of skeletal muscle in <i>mdx-C</i> mice	64
Figure 6.3 Histology of muscles showing decrease in fibrosis and necrosis in 3-wks <i>mdx-C</i> mice	67
Figure 6. 4 Analysis of satellite cells from <i>mdx-C</i> mice	68
Figure 6. 5 Three types of myofibers in <i>mdx-C</i> mice	69
Figure 6. 6 A model for rescue of muscular dystrophy by CRISPR/Cas9-mediated genomic correction	70

List of Tables

	Page
Table 2.1 Comparison of conventional ES cell-based and nuclease-mediated gene targeting in mice	9
Table 2.2. Oligonucleotides and primer sequences	23
Table 2.3. Efficiency of CRISPR/Cas9-mediated genomic editing in wild type mice	24
Table 3.1. Efficiency of CRISPR/Cas9-mediated gene correction in <i>mdx</i> mice	34
Table 4.1. Sequences of the target site (<i>Dmd</i> exon 23) and 32 potential off-target (OT) sites in the mouse genome	40
Table 4.2 Primers for OT analysis	41
Table 4.3. Deep sequencing results of PCR products from the <i>Dmd</i> target site	43
Table 4.4. Deep sequencing results of PCR products from 32 potential off-target regions	44
Table 5.1. Serum creatine kinase (CK) levels and forelimb grip strength of wild-type, <i>mdx</i> and <i>mdx-C</i> mice	57

List of Abbreviations

AAV	adeno-associated virus
Cas	CRISPR associated
CK	creatine kinase
CRISPR	clustered regularly interspaced short palindromic repeat
DMD	Duchenne muscular dystrophy
<i>Dmd</i>	dystrophin gene (mouse)
DSB	double-strand break
HDR	homology-directed repair
indel	insertion/deletion
<i>mdx</i>	X-linked muscular dystrophy
<i>mdx-C</i>	“corrected” <i>mdx</i>
mRNA	messenger ribonucleic acid
NHEJ	non-homologous end-joining
PAM	protospacer adjacent motif
PCR	polymerase chain reaction
RFLP	restriction fragment length polymorphism
sgRNA	single-guide RNA
ssODN	single-stranded oligodeoxynucleotide
T7E1	T7 endonuclease I

Chapter 1 General Introduction

1.1 Introduction of DMD and dystrophin

Skeletal muscle comprises the largest organ system in the human body. It plays a major role in locomotion, metabolism and overall health. Muscular dystrophy (MD) is a group of inherited diseases that are characterized by progressive muscle weakness. There are more than 30 forms of MDs including the following nine major forms: Duchenne, Becker, myotonic, limb-girdle, facioscapulohumeral, congenital, oculopharyngeal, distal and Emery-Dreifuss (Emery, 2002). Different types of MD affect specific groups of muscles, while other organs, such as heart and brain, are also affected in some forms of MD.

Duchenne muscular dystrophy (DMD), which was first described by Duchenne de Boulogne (1806-1875) in 1860s, is one of the most severe and common type of these disease. DMD is caused by mutations in the gene for dystrophin (*DMD*) on the X chromosome and affects approximately 1 in 3,500 boys (Hoffman et al., 1987; Monaco et al., 1986). Dystrophin is a large cytoskeletal structural protein essential for muscle cell membrane integrity. Without it, muscles degenerate, causing weakness and myopathy (Fairclough et al., 2013). Symptoms can be visible between 1 to 6 years old. Most DMD patients are confined to a wheelchair by age 12. Death of DMD patients usually occurs by age 25, typically from breathing complications and cardiomyopathy. Hence, therapy for DMD necessitates sustained rescue of skeletal, respiratory and cardiac muscle structure and function.

DMD arises from a monogenic mutations in dystrophin gene (*DMD*). This makes DMD an ideal disease model for gene therapy. However, the complexity of the *DMD* gene sets a very high threshold for the therapeutic strategy. *DMD* is the largest known gene in the human genome: 2.6 million base pairs which contains 79 exons (**Figure 1A**). Multiple tissue specific promoters control

the expression of the dystrophin isoforms and splice variants (**Figure 1B**). Three independently regulated promoters Dp427b (brain), Dp427m (muscle) and Dp427p (purkinje cells) control the expression of the full length dystrophin, while four internal tissue-specific promoters: Dp260r (retina), Dp140b3 (central nervous system and kidney), Dp116s (Schwann cells) and Dp71g (general) generate amino-terminally truncated forms of dystrophin which also play important roles in the respective tissues (Sadoulet-Puccio and Kunkel, 1996).

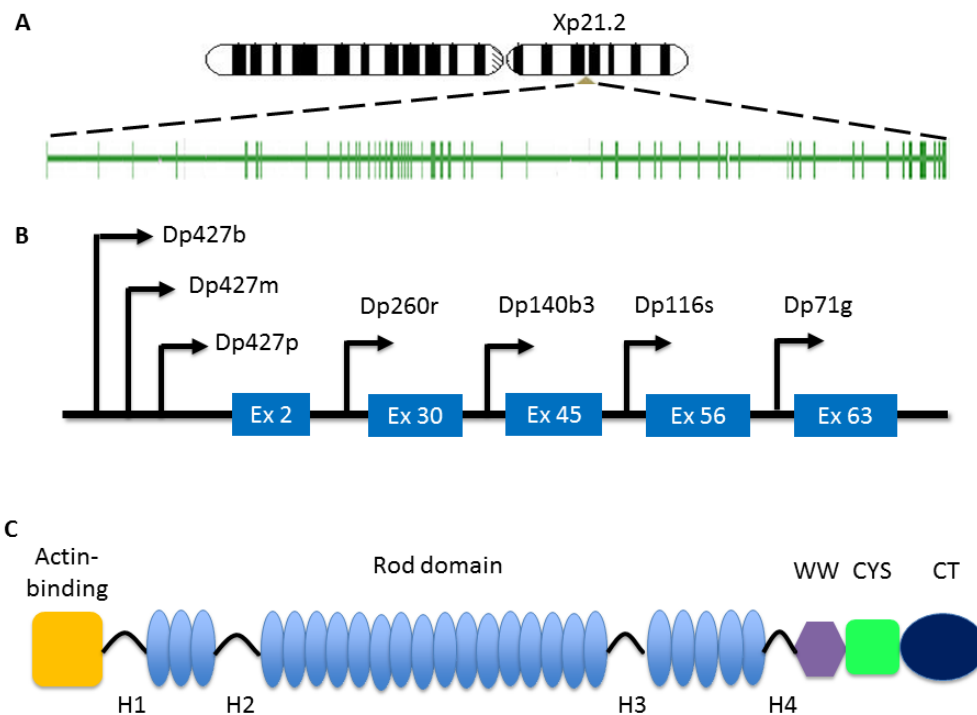


Figure 1.1 Schematic of the exons of human *DMD* and protein domains of dystrophin. (A) The dystrophin gene (*DMD*) which has been identified on chromosome X (Xp21.2) contains 79 exons (B) Multiple tissue-specific promoters regulate the expression of full-length and N-terminal truncated isoforms of dystrophin. (C) Dystrophin is a rod-shaped protein which has four structural domains: actin-binding domain, central rod domain, Cysteine-rich domain (CYS) and carboxy-terminal domain (CT).

Although DMD is inherited in an X-linked recessive pattern, the large size and complicated structure of the *DMD* gene also contribute to its high rate of spontaneous mutation. There are approximately 3000 mutations documented, which contains large deletions or duplications (~77%), small indel. (~12%) and point mutations (~9%).

1.2 Introduction of gene- or cell-based therapies

Since the genetic cause of DMD was identified nearly three decades ago (Worton and Thompson, 1988), several gene- and cell-based therapies have been developed to deliver functional *Dmd* alleles or dystrophin-like protein to diseased muscle tissue (van Deutekom and van Ommen, 2003). These approaches included: 1) dystrophin gene delivery by viral vectors, 2) read-through translation of stop codons by drugs, 3) Oligonucleotide-mediate exon skipping to restore the dystrophin reading frame, 4) up-regulation of the compensatory utrophin gene, and 5) transplantation of normal myoblasts and stem cells.

Despite exciting progress with these treatments, there are major limitations and setbacks. The recent announcement of a phase III trial failure with exon skipping approaches was a disappointment to the DMD community (Wood, 2013). All of these approaches have failed, and none actually correct the primary genetic lesion responsible for the disease. Numerous therapeutic challenges have been encountered and no curative treatment exists (van Deutekom and van Ommen, 2003). In this respect, there is a need for alternative approaches to ameliorate DMD.

1.3 Introduction of CRISPR/Cas9 system

A major breakthrough in genome engineering, RNA-guided nucleases-mediated genome editing, based on Type II CRISPR (Clustered Regularly Interspaced Short Palindromic Repeat)/Cas (CRISPR Associated) systems, offers a new approach to alter the genome (Cong et al., 2013; Jinek et al., 2012; Mali et al., 2013c). In brief, Cas9, a nuclease guided by single-guide RNA (sgRNA), binds to a targeted genomic locus next to the protospacer adjacent motif (PAM) and generates a double-strand break (DSB) **Figure 1.2**. The DSB is then repaired either by non-homologous end-joining (NHEJ), which leads to insertion/deletion (indel) mutations, or by homology-directed repair (HDR), which requires an exogenous template and can generate a precise modification at a target locus (Mali et al., 2013b) (**Figure 1.3**).

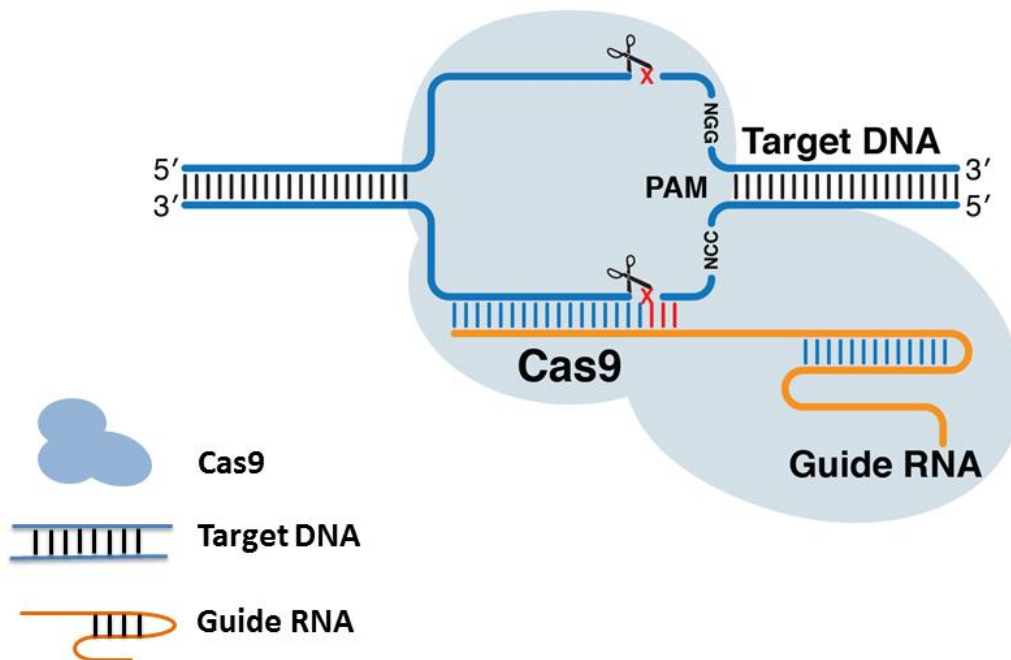


Figure 1.2 Schematic outline of CRISPR/Cas9-mediated genomic targeting.

Cas9 protein (indicated in light blue) guided by guide RNA binds to a target DNA site next to the protospacer adjacent motif (PAM). Red “X” indicates Cas9 cleavage site. Brown lines mark the guide RNA scaffold.

Unlike other gene therapy methods, which add a functional, or partially functional, copy of a gene to a patient's cells but retain the original dysfunctional copy of the gene, this system can remove the defect. Several papers recently demonstrated genetic correction using the CRISPR/Cas9 system in tissue culture cells (Schwank et al., 2013), in mouse germline (Wu et al., 2013), in the rat germline (Yoshimi et al., 2014) and in adult mice (Xue et al., 2014; Yin et al., 2014). However, previous efforts focused on either disease-associated phenotypes in rodents (rather than human diseases) or inherited diseases that are rare and treatable (e.g. tyrosinemia) (Paulk et al., 2010). To the best of our knowledge, correction of a relatively common and currently incurable human genetic disease, such as DMD which is described in our study, by the CRISPR/Cas9 system in animals has not yet been reported.

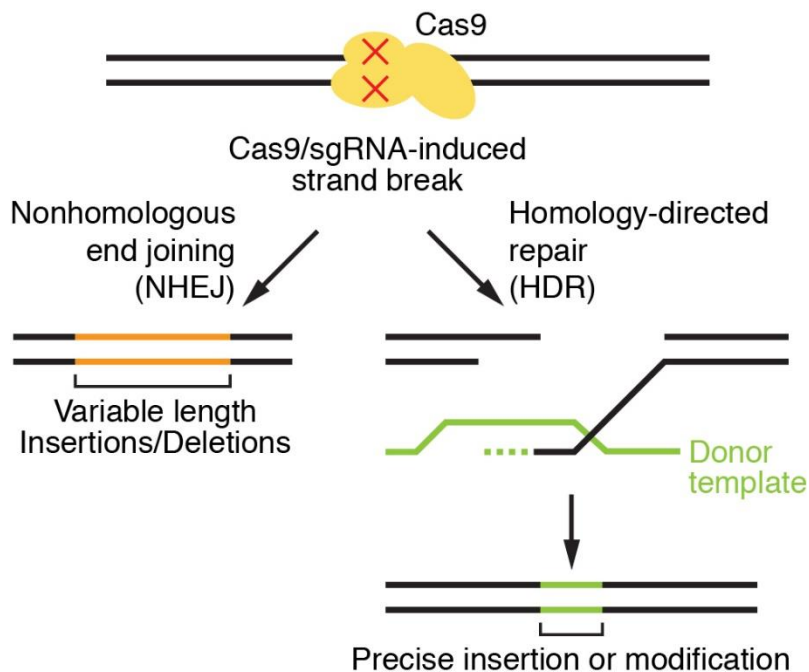


Figure 1.3 Nuclease-induced genome editing

Chapter 2 CRISPR/Cas9-mediated gene editing in mice

2.1 Introduction

Mice with genetic modifications are widely used in basic biological and medical research to understand gene functions and the mechanism of disease (Guan et al., 2010). Traditional gene targeting methods in mice introduce the desired genetic modifications (deletion, insertion or replacement) in mouse embryonic stem (ES) cells through homologous recombination (HR). The targeted ES cells are screened by the positive/negative selection method and identified by Southern blot analysis and/or PCR-based methods. The verified targeted ES cells are injected into wild type mouse blastocysts to generate chimeric mice. If the injected ES cells contribute to the germ line of the chimeric mice, the progeny will contain the genetic modifications (Hall et al., 2009). Despite the fact that this strategy has successfully generated the majority of genetic modified mouse models and offered unprecedented insight into human diseases in the past two decades, the ES cells-based method is a complex, costly, time-consuming and labor-intensive procedure. In the post-genomic era, faster and simpler methods are desirable and necessary.

Multiple engineered nucleases, including meganucleases (MNs) (Posfai et al., 1999), Zinc finger nucleases (ZFNs) (Kim et al., 2010; Kim et al., 1996), transcription-activator like effector nucleases (TALENs) (Christian et al., 2010) and CRISPR/Cas9 system (Cong et al., 2013; Mali et al., 2013c) were developed in the past few years as alternative methods to modify genome of mice and other animal models. These site-specific nucleases have a much higher efficiency of generating DSB at the target sites, while traditional ES cell-based methods depend on spontaneous DSB and HR, which have a low frequency. mRNA or DNA coding for the engineered nuclease system are injected into the one-cell embryo with or without a donor plasmid as a HDR template. Compared to the classical methods, this approach is much simpler and faster (**Table 2.1**).

Additionally, it does not depend on ES cells, which are not readily available in most mammalian animal models, such as the rat.

Table 2.1 Comparison of conventional ES cell-based and nuclease-mediated gene targeting in mice (Wei et al., 2013)

	ES Cell	TALEN	CRISPR/Cas9
Designed component	DNA	Protein	RNA
Essential components	Targeting vector	TALE-Fok I fusion protein	Guide RNA and Cas9
Time consumption for construction	1 month	5~14days	1~3 days
Targeting principle	Homologous recombination	Protein-DNA specific recognition	Watson-Crick complementary rule
Off-target effects	Minor effects	Minor effects	High (?) (Cas9, in vitro) Low (Cas9, in vivo) Low (Cas9 nickase)
Target site availability	No restriction	No restriction	PAM (NGG/NAG) motif restriction
Work in pair/dimmer	Two recombination arms	Yes	No (Cas9)/ Yes (nickase)
Efficiency in mice	Very Low ~1%	High but variable 10~40%	High but variable ~50%
Inheritability in animals	Yes	Yes	Yes
Multitask	No	Not determined	Yes
Target DNA length	Knockout arms ~kb	~2X17 bp + spacer (14~18 bp)	~20 bp Cas9/ ~40bp nickase

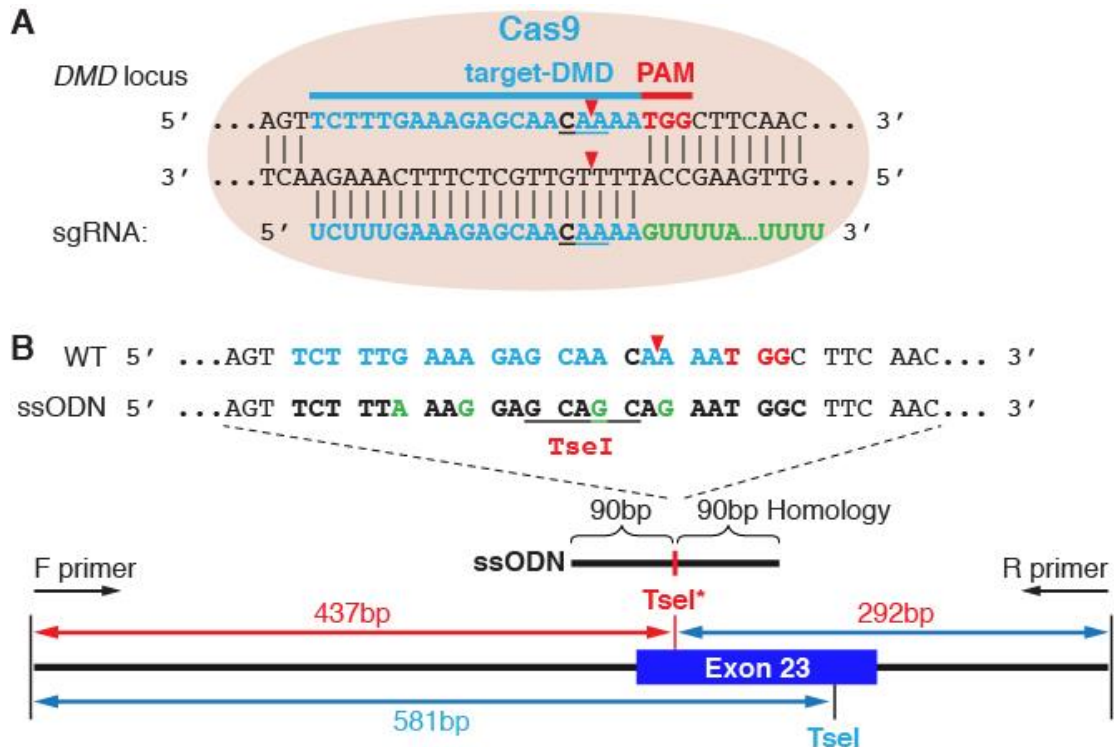


Figure 2.1. Design of guide RNA and HDR template.

(A) Schematic of the 20-nt sgRNA target sequence of *Dmd* (blue) and the PAM (red). Red arrowhead indicates Cas9 cleavage site. Green nucleotides mark the sgRNA scaffold.

(B) Strategy of PCR-based genotyping. ssODN, which contains 90 bp of homology sequence flanking each side of the target site was used as HDR template. ssODN incorporates four silent mutations (green) that eliminate re-cutting by the sgRNA/Cas9 complex and adds a TseI restriction enzyme site (underlined) for genotyping and quantification of HDR-mediated gene editing. Black arrows indicate the positions of the PCR primers corresponding to the *Dmd* gene editing site. Digestion of the PCR product (729 bp) with TseI reveals the occurrence of HDR (437 bp).

2.2 Design and synthesis of Cas9, gRNA and HDR template

We designed a sgRNA to target *Dmd* exon 23 (**Figure 2.1A**) and two single-stranded oligodeoxynucleotide (ssODN) as the templates for HDR-mediated gene repair (**Figure 2.1B**). ssODNs containing 90 bp of homology sequence flanking each side of the target site was used as HDR template. ssODNs also incorporate four silent mutations that eliminate re-cutting by the sgRNA/Cas9 complex and adds a AclI or TseI restriction enzyme site for genotyping and quantification of HDR-mediated gene editing.

We constructed a hCas9 expression vector for in vitro transcription of hCas9 mRNA by subcloning human codon optimized Cas9 gene with T3 promoter into an expression vector (termed T3-hCas9) (**Figure 2.2A**). We linearized and purified the T3-hCas9 plasmid which was used as the template for in vitro transcription. Purified hCas9 mRNA was tested on 1% formaldehyde-agarose (FA) gel (**Figure 2.2B**). A 20 nt target sequence was cloned into a gRNA Cloning Vector plasmid containing the backbone of sgRNA. T7 promoter sequence was added to the sgRNA template by PCR (**Figure 2.2A**). The gel purified PCR products were used as template for in vitro transcription. Purified sgRNA was tested on 6% TBE-Urea gel stained with ethidium bromide (EtBr) (**Figure 2.2C**). The integrity and quality of mRNA and guide RNA is critical for the experiment results. 180nt ssODNs were ordered from Integrated DNA Technologies (Ultramer oligos) without purification, because the PAGE purification process might introduce trace chemical contaminants that reduce embryo viability. Theoretically, longer homology arms might increase the efficiency of HR, however, it has been reported that an optimal HDR efficiency was obtained with a short ssODN (90nt) (Yang et al., 2013b).

Initially, we tested the feasibility and optimized the conditions of CRISPR/Cas9-mediated *Dmd* gene editing in the blastocyst of wild-type mice (C57BL6/C3H and C57BL/6)

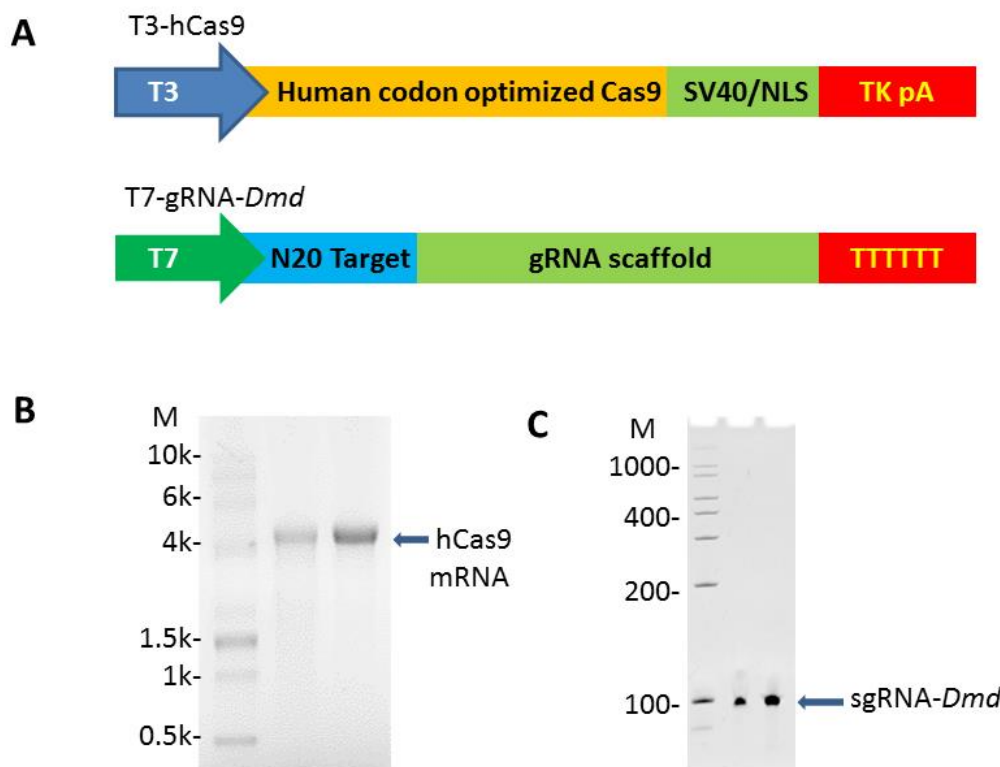


Figure 2.2 Design and synthesis of Cas9 mRNA and guide RNA (A) Schematic illustration of in vitro transcription template for Cas9 and guide RNA. (B) Purified 4.2k hCas9 mRNA (0.5 μ g and 1.0 μ g) was tested on 1% formaldehyde-agarose gel. (C) Purified 102nt sgRNA (0.5 μ g and 1.0 μ g) was tested on 6% TBE-Urea gel stained with ethidium bromide (EtBr). M denotes size marker lane.

2.3 Optimization of the single blastocyst assay

For optimization of the CRISPR/Cas9 system, a fast, sensitive and reproducible assay is required. DNA from culture cell systems or biopsy samples from new born mice are usually assessed and analyzed. However, in vitro culture cell systems do not reflect the in vivo chromatin features and micro-injection of mouse eggs and analysis of the pups is time-consuming, usually taking at least one month. We developed a quick pre-implantation stage assay based on a single

blastocyst following the micro-injection of Cas9 mRNA, sgRNA and ssODNs. Four days after injection, a single mouse blastocyst was used as a genomic DNA for the mutational assay. Polymerase chain reaction (PCR) products corresponding to *Dmd* exon 23 from injected blastocysts were digested with the knock-in restriction enzyme site (AclI) for restriction fragment length polymorphism (RFLP) analysis to screen for HDR (**Figure 2.3**). PCR products corresponding to *Dmd* exon 23 from positive blastocysts were sequenced.

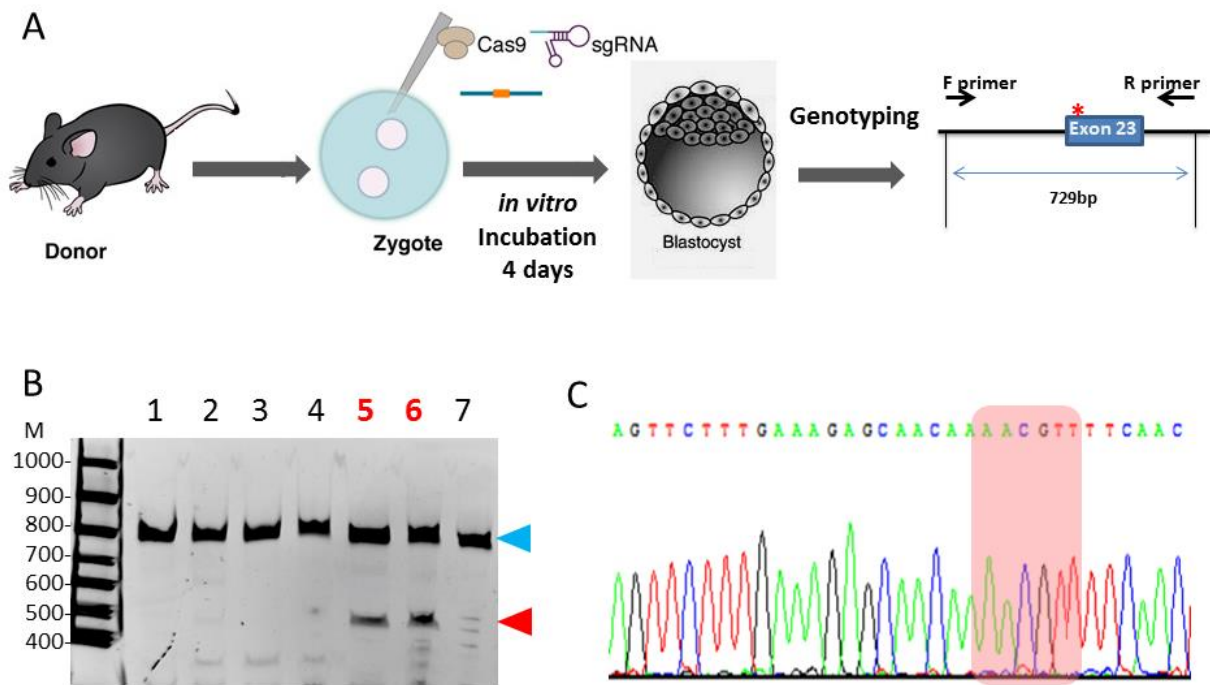


Figure 2.3 A single mouse blastocyst assay for detection of CRISPR/Cas9

(A) Schematic illustration of a single blastocyst assay (B) The PCR products were cut with AclI for RFLP analysis to screen for HDR caused by CRISPR/Cas9-mediated genome editing. DNA products were loaded on a 4-12% TBE gel. Red arrowhead indicates cleavage bands of restriction enzyme. M denotes size marker lane. (C) Sequencing results of PCR products corresponding to *Dmd* exon 23 from a positive blastocyst. Red box indicates the knock-in site.

2.4 CRISPR/Cas9-mediated gene editing in mice

To achieve high genome-editing efficiency and reduce or avoid potential off-target effects, we optimized conditions of CRISPR/Cas9-mediated genomic editing by varying Cas9 mRNA, sgRNA and ssODN concentrations and microinjection methods. We surmised that very low doses of Cas9/sgRNA complexes would fail to efficiently edit targeted sites, however, high amounts of the Cas9/sgRNA complex might also cause off-target effects or arrest embryo development. It has been reported that the ratio between Cas9 mRNA and sgRNA is critical for efficient targeting (Fujii et al., 2013). The method and location of the microinjection also needed to be optimized. Cas9/sgRNA can be injected into the pronuclei and/or cytoplasm of one-cell embryos. Injecting into the cytoplasm tolerates a larger injection volume than with pronuclear injection. Different doses of Cas9 mRNA, sgRNA and ssODNs were injected into wild-type zygote pronuclei and cytoplasm (Nuc+Cyt) or pronuclei only (Nuc) (**Table 2.1**). The injected zygotes were implanted into pseudopregnant female mice. Approximately 50% of the implanted zygotes developed into pups, indicating low toxicity of the injected Cas9/sgRNA.

The wild-type zygotes were co-injected with Cas9 mRNA, sgRNA-DMD and ssODN and then implanted into pseudopregnant female mice. Polymerase chain reaction (PCR) products corresponding to *Dmd* exon 23 from progeny mice were cut with TseI for restriction fragment length polymorphism (RFLP) analysis to screen for HDR. T7 endonuclease I (T7E1), which is specific to heteroduplex DNA caused by CRISPR/Cas9-mediated genome editing, was used to screen for mutations (**Figure 2.4 and 2.5**).

PCR products corresponding to *Dmd* exon 23 from positive progeny mice were sequenced (**Figure 2.6**). Efficiency of CRISPR/Cas9-mediated *Dmd* gene editing is shown in **Table 2.2**.

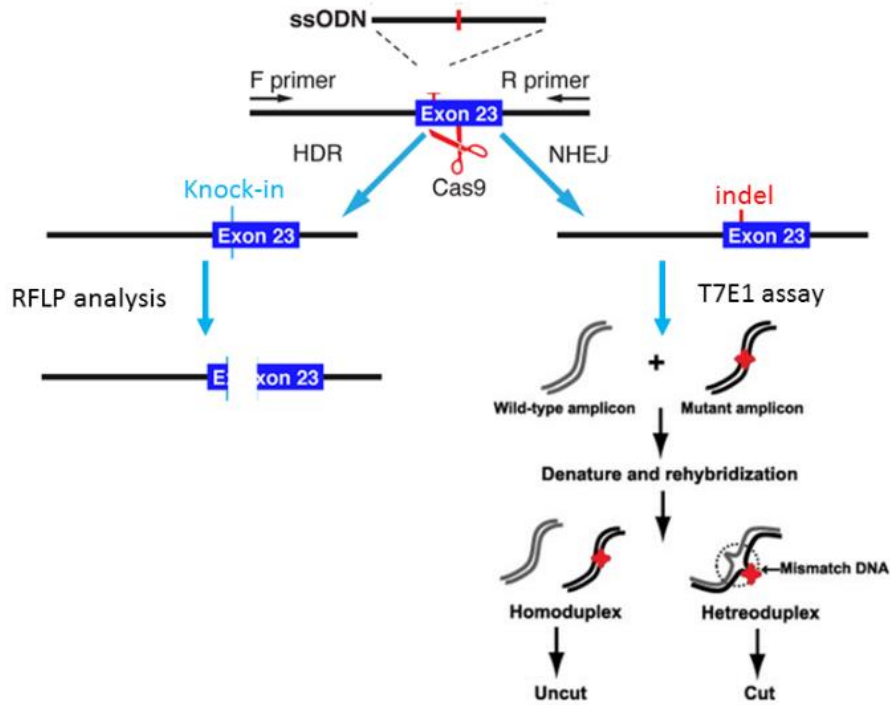


Figure 2.4 Schematic of the PCR-based genotyping. The PCR products corresponding to *Dmd* exon 23 were cut with knock-in enzyme site for restriction fragment length polymorphism (RFLP) analysis to screen for HDR. (Left panel). T7 endonuclease I (T7E1), which is specific to heteroduplex DNA caused by CRISPR/Cas9-mediated genome editing, was used to screen for indel mutations.

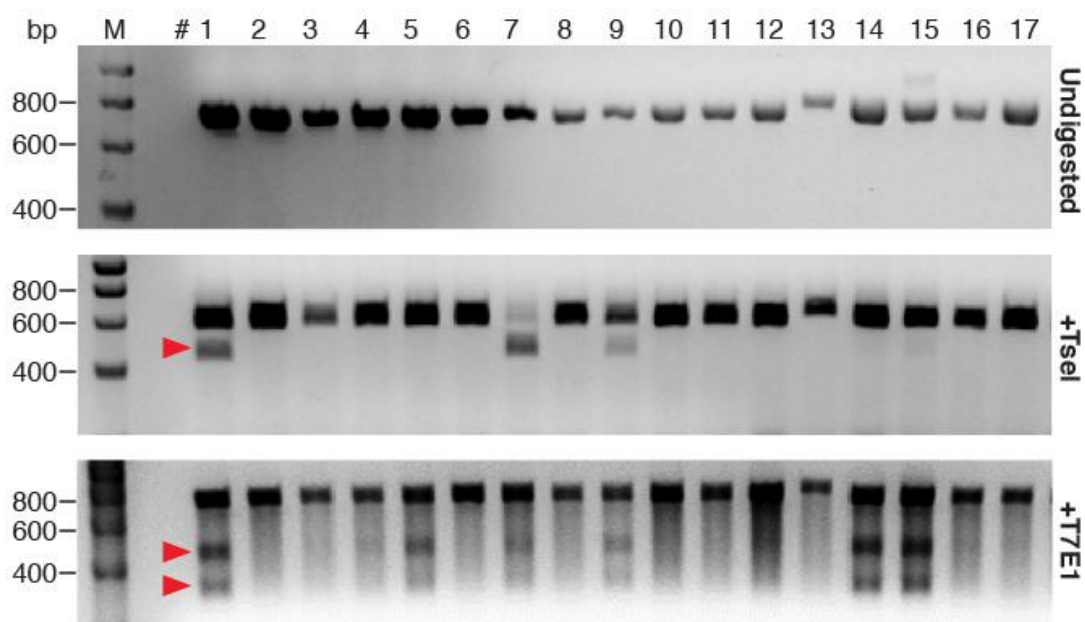


Figure 2.5 PCR-based genotyping in edited mice. (Upper panel) PCR-based genotyping using DNA isolated from tail biopsies of 17 mouse pups from one litter (**Table 2**) with primers listed in **table S1**. (Middle panel) The PCR products were cut with TseI for restriction fragment length polymorphism (RFLP) analysis to screen for HDR. (Lower panel) T7 endonuclease I (T7E1), which is specific to heteroduplex DNA caused by CRISPR/Cas9-mediated genome editing, was used to screen for mutations. DNA products were loaded on a 2% agarose gel. Red arrowhead indicates cleavage bands of TseI or T7E1. M denotes size marker lane. bp indicates the base pair length of the marker bands.

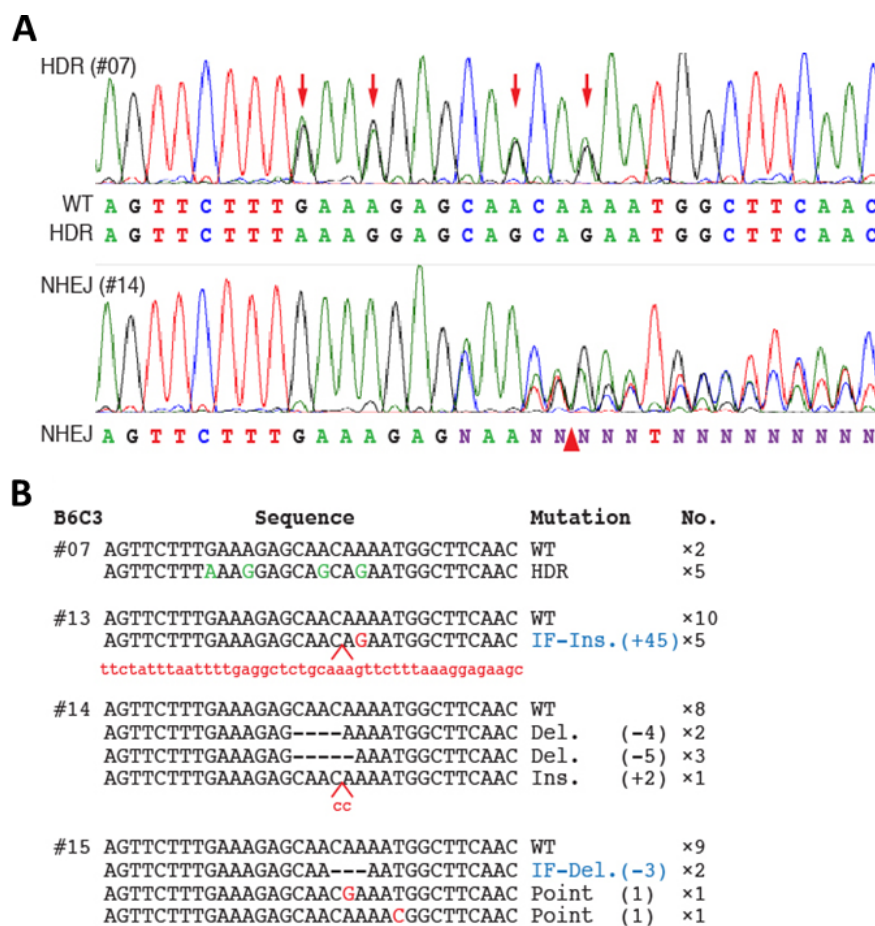


Figure 2.6 Sequencing results of PCR products from positive progeny mice (A) Sequencing results of PCR product of (upper panel) mouse #07 (from **Figure 2.5**) showing HDR and of (lower panel) mouse #14 (from **Figure 2.5**) showing NHEJ-mediated editing of the *Dmd* gene. Red arrows indicate the location of the point mutations introduced by HDR. Red arrowhead points to the mixed sequencing peaks on chromatograms near the targeted site indicating heterozygous NHEJ-mediated gene editing. **(B)** Sequence of *Dmd* alleles from four F₀ mice (#07, #13, #14 and #15 from **Figure 2.5**) from microinjection of Cas9, sgRNA and ssODN into B6C3F1 mouse zygotes. PCR products from genomic tail DNA of each mouse

were subcloned into pCRII-TOPO vector and individual clones were picked and sequenced. Silent mutations are indicated with green letters. Point mutations are indicated with red letters. Red lower case letters are the inserted sequences at the site indicated by the red arrowhead. Deleted sequences are replaced by black dashes. The genotype of each genomic DNA clone is listed next to the sequence and in-frame insertions or deletions are labeled in blue (termed IF-Ins. and IF-Del.). The number of inserted nucleotides is indicated by (+) and the deletion is indicated with (-). The number (No.) of clones with identical sequence is indicated by (×).

2.5 Materials and Methods

2.5.1 Plasmids.

The hCas9 plasmid (Addgene plasmid 41815) containing the human codon optimized Cas9 gene and the gRNA Cloning Vector plasmid (Addgene plasmid 41824) containing the backbone of sgRNA were purchased from Addgene. Cloning of sgRNA was done according to the Church Lab CRISPR plasmid instructions (<http://www.addgene.org/crispr/church/>).

2.5.2 In vitro transcription of Cas9 mRNA and sgRNA.

T3 promoter sequence was added to the hCas9 coding region by PCR. T3-hCas9 PCR product was gel purified and subcloned into pCRII-TOPO vector (Invitrogen) according to the manufacturer's instructions. Linearized T3-hCas9 plasmid was used as the template for in vitro transcription using the mMESSAGE mMACHINE T3 Transcription Kit (Life Technologies). T7 promoter sequence was added to the sgRNA template by PCR. The gel purified PCR products were used as template for in vitro transcription using the MEGAscript T7 Kit (Life Technologies). hCas9 RNA and sgRNA were purified by MEGAclear kit (Life Technologies) and eluted with nuclease-free water (Ambion). The concentration of RNA was measured by a NanoDrop instrument (Thermo Scientific).

2.5.3 Single-stranded oligodeoxynucleotide (ssODN).

ssODN was used as HDR template and purchased from Integrated DNA Technologies as Ultramer DNA Oligonucleotides. ssODN was mixed with Cas9 mRNA and sgRNA directly without purification. The sequence of ssODN is listed in **Table 2.2**.

2.5.4 CRISPR/Cas9-mediated genomic editing by one-cell embryo injection.

All animal procedures were approved by the Institutional Animal Care and Use Committee at the University of Texas Southwestern Medical Center. B6C3F1 (C57BL/6NCr female X C3H/HeN MTV male), C57BL/6NCr were two mouse strains used as oocyte donors. Superovulated female B6C3F1 mice (6 weeks old) were mated to B6C3F1 stud males. Superovulated female C57BL/6NCr females (12-18 grams) were mated to C57BL/6NCr males and superovulated female homozygote C57BL/10ScSn-*Dmd^{mdx}/J* (12-18 grams) were mated to hemizygote C57BL/10ScSn-*Dmd^{mdx}/J* stud males. Zygotes were harvested and kept in M16 medium (Brinster's medium for ovum culture with 100U/ml penicillin and 50 mg/ml streptomycin) at 37°C for 1 hour. Zygotes were transferred to M2 medium (M16 medium and 20 mM HEPES) and injected with hCas9 mRNA, sgRNA and ssODN. Cas9/sgRNA was injected into the pronucleus only (termed Nuc) or pronucleus and cytoplasm (termed Nuc+Cyt). Different doses of Cas9 mRNA, sgRNA and ssODNs were injected into zygotes by Nuc or Nuc+Cyt (as detailed in **table S2**). Injected zygotes were cultured in M16 medium for 1 hour at 37°C and then transferred into the oviducts of pseudopregnant ICR female mice.

2.5.5 DNA extraction from blastocysts.

A single blastocyst was collected into a PCR tube and add to 5 µl of 1mg/ml Protease K in DirectPCR Lysis Reagent (Cell). Crude lysates are incubate at 55 °C for 30 min and then at 85 °C for 15 min. The tubes were centrifuged for 10 second. 2.0 µl of lysate was used for a 50 µl PCR reaction.

2.5.6 Isolation of genomic DNA from tails.

Tail biopsies were added to 100 µl of 25mM NaOH / 0.2 mM EDTA solution and placed at 95 °C for 15 min and then cooled to room temperature. Following the addition of 100 µl of 40 mM Tris-HCl (pH 5.5), the tubes were centrifuged at 15,000 x g for 5 minutes. DNA samples were kept at 4 °C for several weeks or at -20 °C for long-term storage. Genomic DNA was isolated from muscle using TRIzol (Life Technologies) according to the manufacturer's instructions.

2.5.7 Amplifying the target genomic region by PCR.

PCR assays contained 2 µl of GoTaq polymerase (Promega), 20 µl of 5X Green GoTaq Reaction Buffer, 8 µl of 25mM MgCl₂, 2 µl of 10 µM primer (DMD729F and DMD729R) (**Table 2.2**), 2 µl of 10mM dNTP, 8 µl of genomic DNA, and ddH₂O to 100 µl. PCR conditions were: 94 °C for 2 min; 32X (94 °C for 15 sec, 59 °C for 30 sec, 72 °C for 1 min); 72 °C for 7 min; then held at 4 °C. PCR products were analyzed by 2% agarose gel electrophoresis and purified from the gel using the QIAquick PCR Purification Kit (Qiagen) for direct sequencing. These PCR products were subcloned into pCRII-TOPO vector (Invitrogen) according to the manufacturer's instructions. Individual clones were picked and the DNA was sequenced.

2.5.8 RFLP analysis of PCR products.

Digestion reactions consisting of 20 µl of genomic PCR product, 3 µl of 10X NEB buffer CS, and 1 µl of TseI (New England BioLabs) were incubated for 1 hour at 65 °C and analyzed by 2% agarose gel electrophoresis. Digested PCR product from wild-type DNA is 581bp, while HDR-mediated genomic editing DNA from F₀ mice shows an additional product at approximately 437bp.

2.5.9 T7E1 analysis of PCR products.

Mismatched duplex DNA was obtained by denaturation/renaturation of 25 μ l of the genomic PCR samples using the following conditions:

95 $^{\circ}$ C for 10 min,
95 $^{\circ}$ C to 85 $^{\circ}$ C (-2.0 $^{\circ}$ C/s),
85 $^{\circ}$ C for 1 min,
85 $^{\circ}$ C to 75 $^{\circ}$ C (-0.3 $^{\circ}$ C/s),
75 $^{\circ}$ C for 1 min,
75 $^{\circ}$ C to 65 $^{\circ}$ C (-0.3 $^{\circ}$ C/s),
65 $^{\circ}$ C for 1 min,
65 $^{\circ}$ C to 55 $^{\circ}$ C (-0.3 $^{\circ}$ C/s),
55 $^{\circ}$ C for 1 min,
55 $^{\circ}$ C to 45 $^{\circ}$ C (-0.3 $^{\circ}$ C/s),
45 $^{\circ}$ C for 1 min,
45 $^{\circ}$ C to 35 $^{\circ}$ C (-0.3 $^{\circ}$ C/s),
35 $^{\circ}$ C for 1 min,
35 $^{\circ}$ C to 25 $^{\circ}$ C (-0.3 $^{\circ}$ C/s),
25 $^{\circ}$ C for 1 min,
hold at 4 $^{\circ}$ C.

Following denaturation/renaturation, the following was added to the samples: 3 μ l of 10X NEB buffer 2, 0.3 μ l of T7E1 (New England BioLabs), and ddH₂O to 30 μ l. Digested reactions were incubated for 1 hour at 37 $^{\circ}$ C. Undigested PCR samples and T7E1 digested PCR products were analyzed by 2% agarose gel electrophoresis. Undigested PCR product is 729bp, while genomic DNA from F₀ mice with mismatched DNA showed two additional digestion products at approximately 440bp and 290bp.

Table 2.2. Oligonucleotides and primer sequences.

ssODN used for HDR-mediated editing via embryo micro-injection	
Dmd_donor_TseI-s180	TGA TAT GAA TGA AAC TCA TCA AAT ATG CGT GTT AGT GTA AAT GAA CTT CTA TTT AAT TTT GAG GCT CTG CAA AGT TCT TTA AAG GAG CAG CAG AAT GGC TTC AAC TAT CTG AGT GAC ACT GTG AAG GAG ATG GCC AAG AAA GCA CCT TCA GAA ATA TGC CAG AAA TAT CTG TCA GAA TTT
Primers for In vitro transcription	
T3-hCas9-F	gaattgAATTAACCCTCACTAAAGGGagaGCCACCATG GAC AAG AAG TAC TCC ATT G
hCas9-stop-R	TCA CAC CTT CCT CTT CTT CTT GGG GTC AGC
Dmd_gRNA-wtG	ttaatacgactcactatag GTCT TTG AAA GAG CAA CAA AA
Dmd_gRNA-mdxG	ttaatacgactcactatag GTCT TTG AAA GAG CAA TAA AA
gRNA-R2	aaaagcaccgactcggtgccac
Primers for genotyping	
Dmd_729F	gagaaacttctgtgatgtgaggacata
Dmd_729R	caatatcttgaaggactctgggtaaa

Table 2.3. Efficiency of CRISPR/Cas9-mediated genomic editing in wild type mice by cytoplasm and pronuclear injection.

Strain	Dose of Injection Cas9/sgRNA/ssODN (ng/ μ l)	Injection Methods	No. of Transferred Zygotes	No. of Pups/ Zygotes (%)	No. of Mutant Founders/Pups (%)	No. of HDR/ Pups (%)
C57BL6/C3H	5/2.5/5	Nuc	60	29 (48%)	9 (31%)	1 (3.4%)
		Nuc+Cyt	60	27 (45%)	5 (19%)	1 (3.7%)
	10/5/5	Nuc	30	13 (43%)	1(7.7%)	1 (7.7%)
		Nuc+Cyt	30	17 (57%)	6(35%)	3 (18%)
C57BL/6	10/5/10	Nuc	48	9 (18%)	3 (33%)	1 (11%)
	50/20/10	Nuc+Cyt	30	12 (40%)	1 (8.3%)	0

Chapter 3 CRISPR/Cas9-mediated gene correction in *mdx* mice

3.1 Introduction

Animal models have been used for many decades to understand basic biological systems and to initiate clinically significant studies. The most studied animal model of DMD is the X-linked murine muscular dystrophy, *mdx* mouse discovered in 1981 by screening of mouse serum enzymes (Bulfield et al., 1984). It was confirmed in both human and mouse that the mutations of muscular dystrophy lie in the dystrophin gene (Hoffman et al., 1987; Monaco et al., 1986). Four new mutations of *Dmd*, termed *Dmd*^{*mdx2cv*} to *Dmd*^{*mdx5cv*} were identified from the progeny of chemical mutagen-treated male mice by screening the elevated plasma creatine kinase level.

The *mdx* mouse contains a spontaneous nonsense mutation (C to T) in exon 23 of the *Dmd* gene (Banks and Chamberlain, 2008) (Figure 3.1). The *mdx*^{2CV} mouse has a mutation (A to T) in the intron 42/exon 43 splice acceptor site which induces aberrant splice products. The *mdx*^{3CV} model results from a mutant (T to A) in the intron 65 which creates a novel splice acceptor upstream of the natural site in exon 66. Aberrant splicing results in the inclusion of 14 bp of intronic sequence and shifts the reading frame. The *mdx*^{4CV} allele has a C to T transition in exon 53 which creates a premature stop codon. The *mdx*^{5CV} mouse has an A to T mutation in exon 10, which creates a new splice donor site in the middle of this exon and creates a frame shifting deletion (53 bp). In addition, the *mdx52* mouse was also generated by deletion of exon 52, to simulate the phenotype seen in human patients. All *mdx* mouse models are widely used in the studies of molecular mechanisms of pathogenesis of DMD and to develop the therapeutic strategies (Figure 3.1).

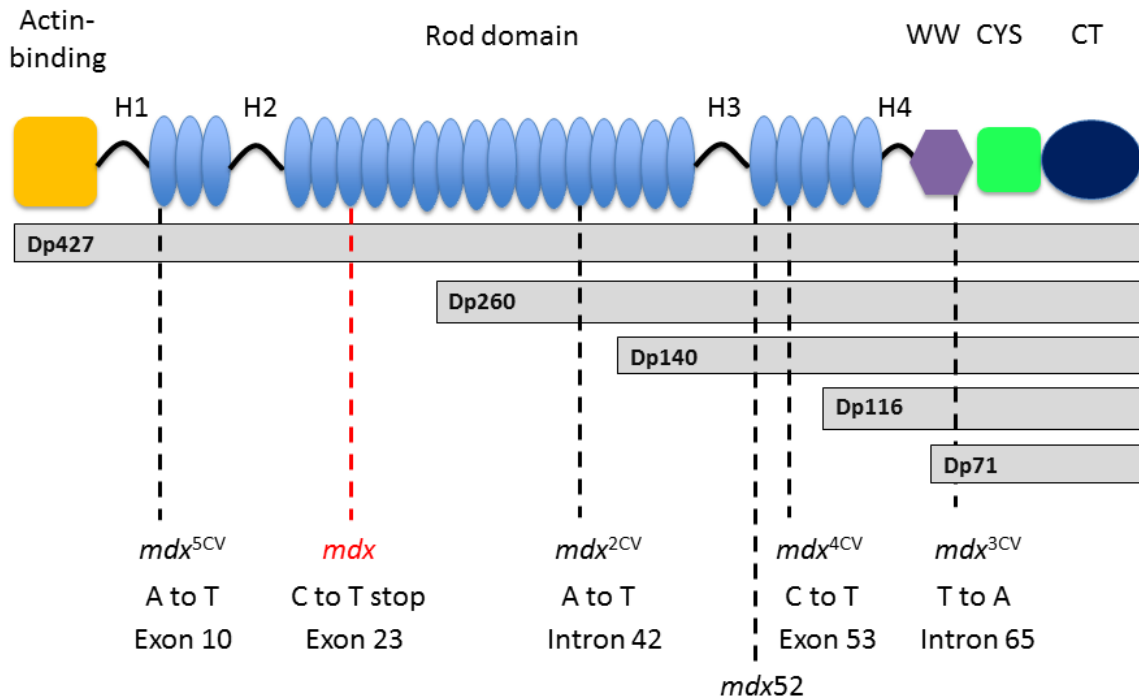


Figure 3.1 The molecular structure of dystrophin isoforms and the position of mutations in *mdx* mouse strains. The dystrophin contains multiple tissue specific promoters which express isoforms with different size, 427kD, 260kD, 140kD, 116kD and 71kD. The position of mutations in the six strain of *mdx* mice are shown below. The different strain of these mice also express different isoforms of dystrophin in non-muscular tissues. For example, *mdx* mouse, labeled in red expresses four other shorter isoforms (260kD, 140kD, 116kD and 71kD).via alternative promoter usage.

3.2 Design and synthesis of Cas9, gRNA-*mdx* and HDR template

The objective of this study was to correct the genetic defect in the *Dmd* gene of *mdx* mouse (C57BL/10ScSn-*Dmd*^{*mdx*/J}) by CRISPR/Cas9-mediated genome editing in vivo. We injected Cas9,

sgRNA and HDR template into mouse zygotes to correct the disease-causing gene mutation in the germ line (**Figure 3.2**) (Wang et al., 2013; Yang et al., 2013a), a strategy that has the potential to correct the mutation in all cells of the body, including myogenic progenitors. Safety and efficacy of CRISPR/Cas9-based gene therapy was also evaluated.

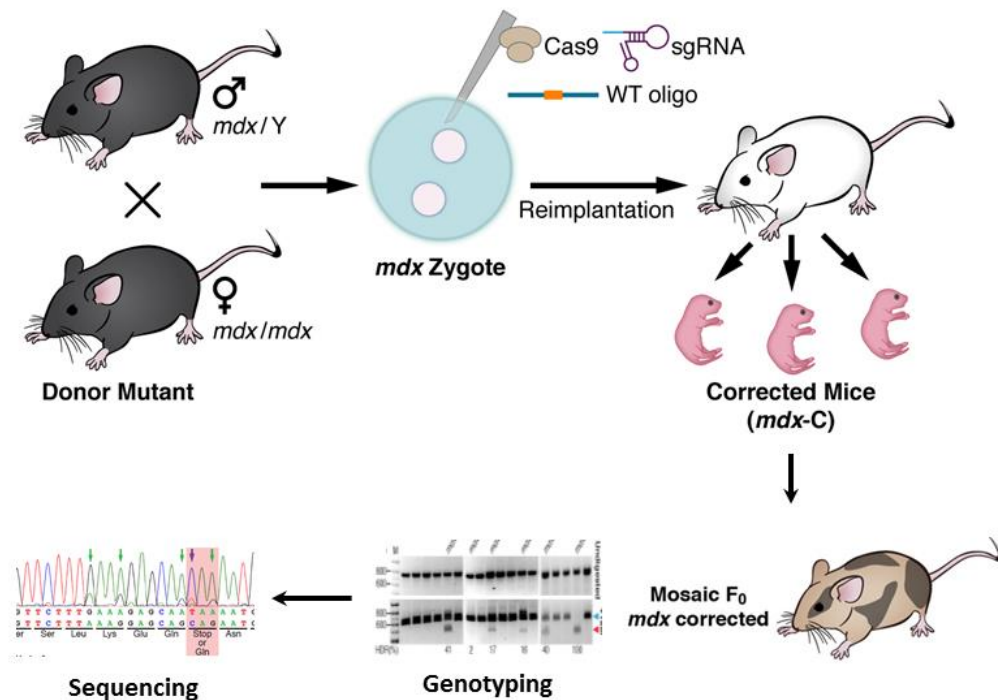


Figure 3.2 Strategy of the gene correction in *mdx* mice via germ line gene therapy. The *mdx* zygotes were co-injected with Cas9 mRNA, sgRNA and ssODN and then implanted into pseudopregnant female mice. “Corrected” F₀ *mdx* progeny (termed *mdx-C*) were identified by PCR-based genotyping.

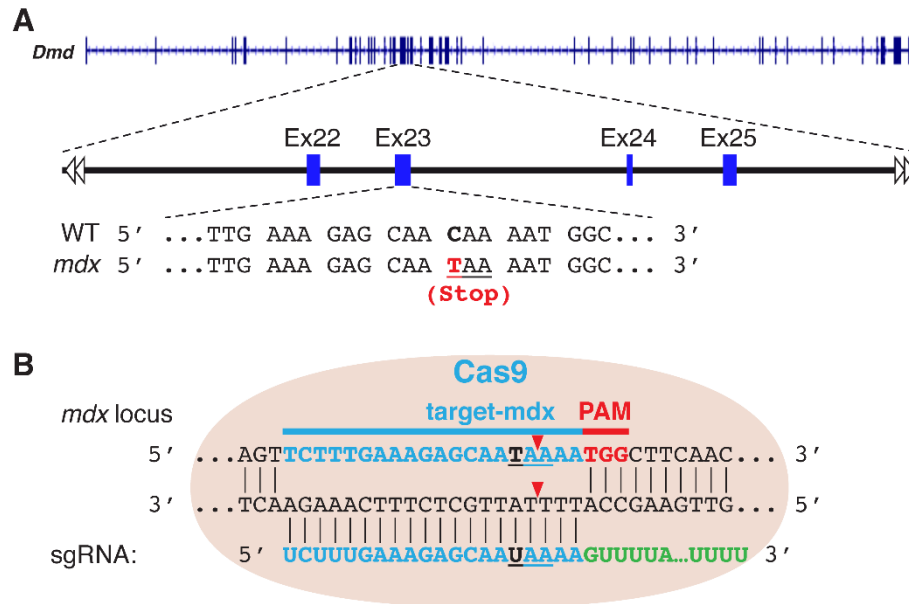


Figure 3.3 CRISPR/Cas9-mediated *Dmd* correction in *mdx* mice.

(A) Schematic of the targeted exon of mouse *Dmd* and sequence from wild-type (upper) and *mdx* mice (lower). The *mdx* point mutation (C to T) is marked in red and the premature stop codon is underlined.

(B) Schematic of the 20-nt sgRNA target sequence of the *mdx* allele (blue) and the PAM (red). Red arrowhead indicates Cas9 cleavage site. ssODN, which contains 90 bp of homology sequence flanking each side of the target site was used as HDR template. ssODN incorporates four silent mutations (green) and adds a TseI restriction enzyme site (underlined) for genotyping and quantification of HDR-mediated gene editing.

3.3 CRISPR/Cas9-mediated gene correction

We next applied the optimized CRISPR/Cas9-mediated genomic editing method to *mdx* mice (**Figure 3.2**). The CRISPR/Cas9-mediated genomic editing system will correct the point mutation in *mdx* mice during embryonic development via HDR or NHEJ (**Figure 3.4**).

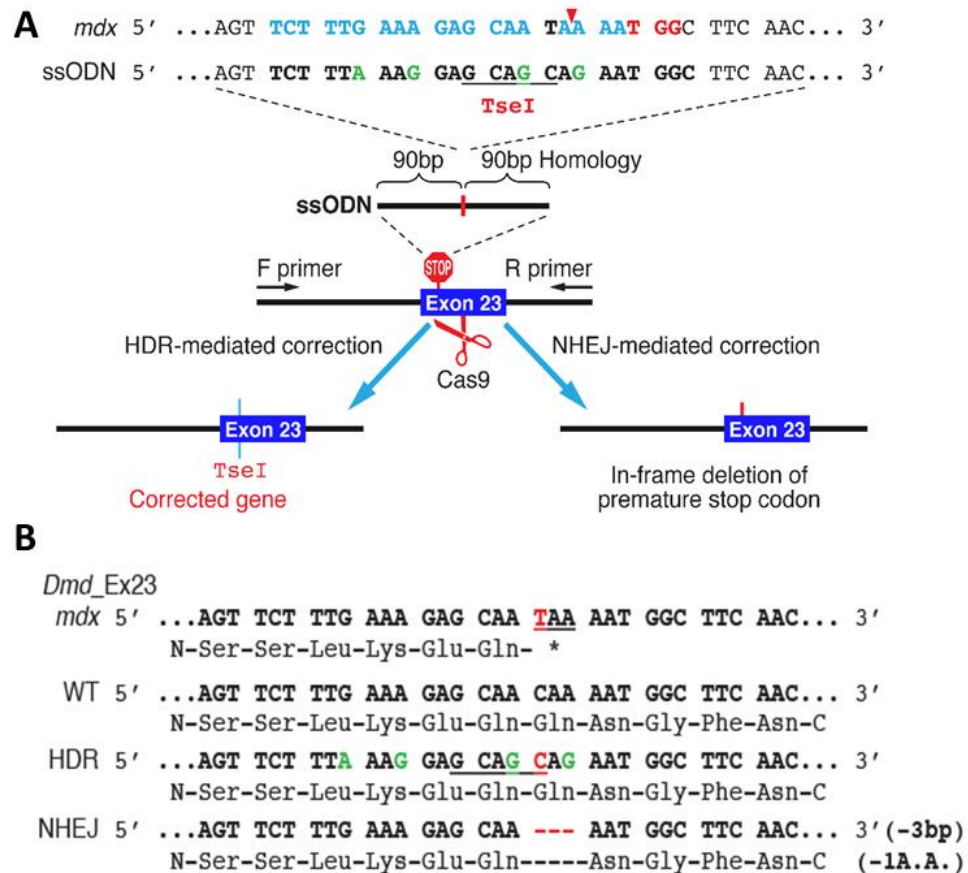


Figure 3.4 Strategy of the gene correction via HDR or NHEJ.

(A) Schematic illustrating CRISPR/Cas9-mediated gene correction via HDR or NHEJ. (B) The corresponding amino acid residues are shown under the DNA sequence

3.4 Genotyping of corrected *mdx* progeny

“Corrected” *mdx* progeny (termed *mdx-C*) were identified by Restriction Fragment Length Polymorphism (RFLP) analysis and the mismatch-specific T7 endonuclease I (T7E1) assay (Figure 3.5).

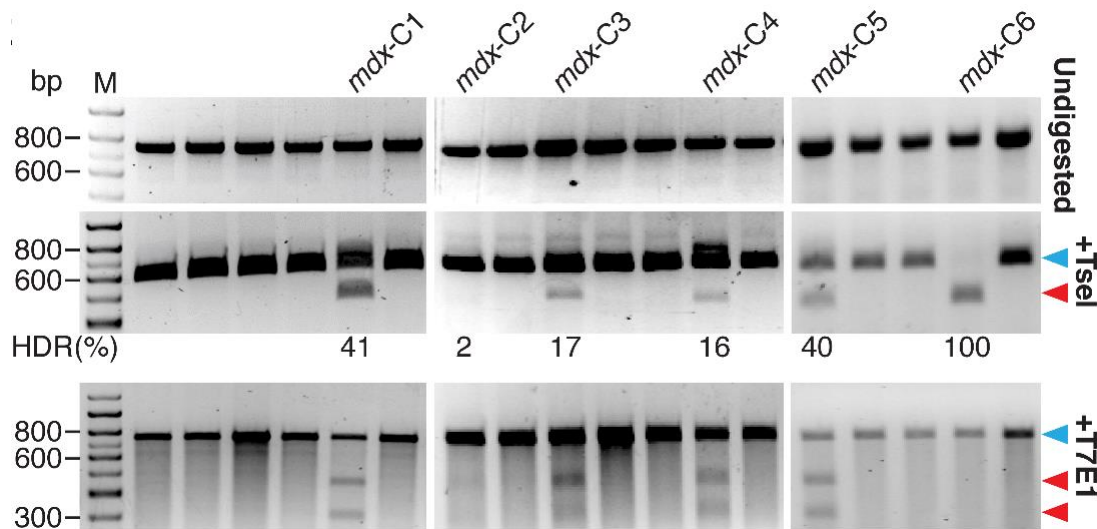


Figure 3.5 Genotyping results of *mdx-C* mice with mosaicism of 2-100% corrected *Dmd* gene. Undigested PCR product (upper panel), TseI digestion (middle panel) and T7E1 digestion (lower panel) on a 2% agarose gel. The red arrowhead in the middle panel marks the DNA band indicating HDR-mediated correction generated by TseI digestion. The blue arrowhead marks the DNA band of the uncorrected *mdx* allele. The relative intensity of the DNA bands (indicated by blue and red arrowheads) reflects the percentage of HDR in the genomic DNA. The percent of HDR is located under the middle panel. The band intensity was quantified by ImageJ (NIH). The blue and red arrowheads in the lower panel indicate uncut and cut bands by T7E1. M denotes size marker lane. bp indicates the base pair length of the marker bands.

3.5 Sequencing of *mdx-C*

We analyzed a total of eleven different *mdx-C* mice. PCR products of *Dmd* exon 23 from seven *mdx-C* mice with HDR-mediated gene correction (termed *mdx-C1* to *C7*) and four *mdx-C* mice containing NHEJ-mediated in-frame deletions of the stop codon (termed *mdx-N1* to *N4*) were sequenced. Sequencing results revealed that CRISPR/Cas9-mediated germline editing produced genetically mosaic *mdx-C* mice displaying from 2 to 100% correction of the *Dmd* gene (**Figure 3.6**). A wide range of mosaicism occurs if CRISPR/Cas9-mediated repair occurs after the zygote stage, resulting in genomic editing in a subset of embryonic cells (Yen et al., 2014). All mouse progeny developed to adults without signs of tumor growth or other abnormal phenotypes.

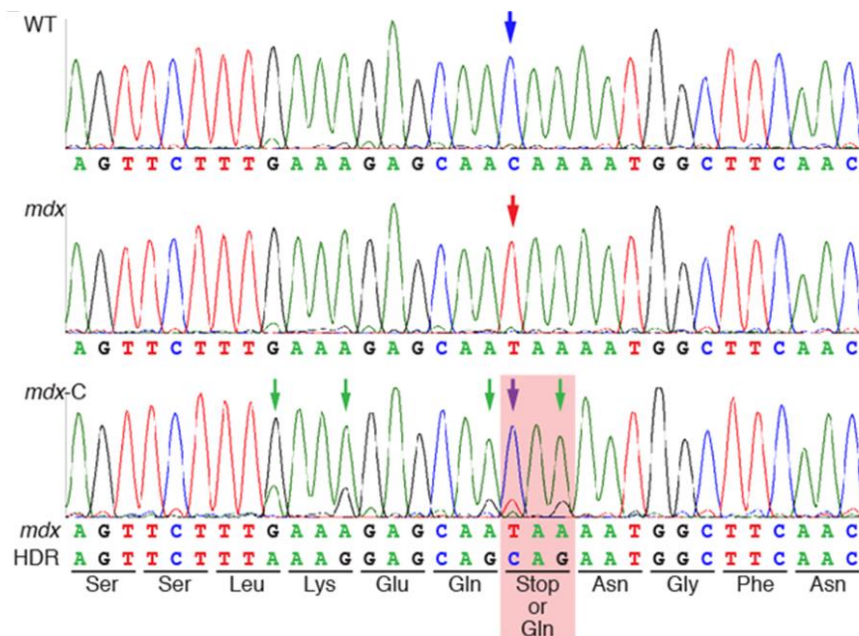


Figure 3.6 Direct sequencing results of WT, *mdx* and corrected *mdx-C* mice. Blue arrow indicates the WT allele (upper). Red arrow indicates the *mdx* allele (middle). Purple arrow indicated the corrected allele mediated by HDR. Green arrows indicate the silent mutation sites (lower). The corresponding amino acid residues are shown under the DNA sequence. Red box indicates the corrected site.

HDR-mediated correction			
	Sequence	Mutation	No.
<i>mdx-C1</i>	AGTTCTTTGAAAGAGCAATAAAATGGCTTCAAC	<i>mdx</i>	×13
	AGTTCTTTAAAGGAGCAGCAGAATGGCTTCAAC	HDR	×12
<i>mdx-C2</i>	AGTTCTTTGAAAGAGCAATAAAATGGCTTCAAC	<i>mdx</i>	×23
	AGTTCTTTAAAGGAGCAGCAGAATGGCTTCAAC	HDR	×1
<i>mdx-C3</i>	AGTTCTTTGAAAGAGCAATAAAATGGCTTCAAC	<i>mdx</i>	×17
	AGTTCTTTAAAGGAGCAGCAGAATGGCTTCAAC	HDR	×5
<i>mdx-C4</i>	AGTTCTTTGAAAGAGCAATAAAATGGCTTCAAC	<i>mdx</i>	×17
	AGTTCTTTAAAGGAGCAGCAGAATGGCTTCAAC	HDR	×5
<i>mdx-C5</i>	AGTTCTTTGAAAGAGCAATAAAATGGCTTCAAC	<i>mdx</i>	×3
	AGTTCTTTAAAGGAGCAGCAGAATGGCTTCAAC	HDR	×3
<i>mdx-C6</i>	AGTTCTTTGAAAGAGCAATAAAATGGCTTCAAC	<i>mdx</i>	×0
	AGTTCTTTAAAGGAGCAGCAGAATGGCTTCAAC	HDR	×6
<i>mdx-C7</i>	AGTTCTTTGAAAGAGCAATAAAATGGCTTCAAC	<i>mdx</i>	×5
	AGTTCTTTAAAGGAGCAGCAGAATGGCTTCAAC	HDR	×4
NHEJ-mediated correction			
<i>mdx-N1</i>	AGTTCTTTGAAAGAGCAATAAAATGGCTTCAAC	<i>mdx</i>	×2
	AGTTCTTTGAA-----TGGCTTCAAC	IF-Del. (-12)	×10 (83%)
<i>mdx-N2</i>	AGTTCTTTGAAAGAGCAATAAAATGGCTTCAAC	<i>mdx</i>	×7
	AGTTCTTTG-----CA---AAATGGCTTCAAC	IF-Del. (-9)	×4 (36%)
<i>mdx-N3</i>	AGTTCTTTGAAAGAGCAATAAAATGGCTTCAAC	<i>mdx</i>	×8
	AGTTCTTTGAAAGA-A-----//-----CCT	IF-Del. (-48)	×2 (20%)
<i>mdx-N4</i>	AGTTCTTTGAAAGAGCAATAAAATGGCTTCAAC	<i>mdx</i>	×3
	AGTTCTTTGAAAGAGCAA---AATGGCTTCAAC	IF-Del. (-3)	×3 (43%)
	AGTTCTTTGAAAGAGTAATAAAAATGGCTTCAAC	Point	×1

Figure 3.7 Sequence of *Dmd* alleles present in F₀ *mdx-C* mice (**Figure 3.5**) from microinjection of Cas9, sgRNA and ssODN into *mdx* mouse (C57BL/10ScSn-*Dmd*^{*mdx*/J}) zygotes. PCR products from genomic tail DNA of each mouse were subcloned into pCRII-TOPO vector and individual clones were picked and sequenced. The *mdx* point mutation (C to T) is marked in red. Silent mutations are indicated with green letters. The number (No.) of clones with identical sequence is indicated by (×). The variability observed in the ratio of HDR or NHEJ sequence to *mdx* sequence for each *mdx-C* mouse reflects the degree of mosaicism.

Table 3.1. Efficiency of CRISPR/Cas9-mediated gene correction in *mdx* mice by cytoplasm and pronuclear injection.

Dose of Injection Cas9/sgRNA/ssODN (ng/ μ l)	Injection Methods	No. of Transferred Zygotes	No. of Pups/Zygotes (%)	No. of Mutant Founders/Pups (%)	No. of HDR /Pups (%)
10/10/10	Nuc	103	29 (28%)	4 (14%)	1 (3.4%)
	Nuc+Cyt	150	58 (39%)	7 (12%)	4 (6.9%)
50/20/10	Nuc	30	14 (47%)	2 (6.7%)	0
	Nuc+Cyt	120	23 (19%)	9 (39%)	2 (8.9%)

3.6 Materials and Methods

CRISPR/Cas9-mediated gene correction by one-cell embryo injection.

All animal procedures were approved by the Institutional Animal Care and Use Committee at the University of Texas Southwestern Medical Center. C57BL/10ScSn-*Dmd*^{*mdx*}/J was used as oocyte donors. Superovulated female homozygote C57BL/10ScSn-*Dmd*^{*mdx*}/J (12-18 grams) were mated to hemizygote C57BL/10ScSn-*Dmd*^{*mdx*}/J stud males.

Chapter 4 Analysis of off-target effects

4.1 Introduction

One key concern for the engineered nucleases, including ZNF, TALENs and CRISPR/Cas, is the specificity of these genome editing tools. Off-target effects may cause unexpected cuts and mutations in the genome site. This issue is important since engineered nucleases are being applied therapeutically to repair mutations in human diseases.

Off-target effects by ZNF and TALENs have been reduced by the requirement that only the formation of heterodimers of the nuclease domains have function. In addition, the target sequence for ZNF and TALENs is usually more than 30bp. In contrast, Cas9 from *Streptococcus pyogenes* which has two nuclease domains only needs a 20nt guide RNA to bind to its target sequence and make a double strand break. It is not surprising that, in CRISPR/Cas9 system, earlier studies have shown that a few mismatches between the guide RNA and its target are tolerated. The following studies from different groups, especially the genome-wide binding of Cas9 and crystal structure of Cas9/gRNA/target DNA, offers a better mechanism of target recognition and target specificity of Cas9 system. Perfect complementarity between target sequence and the 5'-nucleotide seed sequence at the 3' end of the gRNA is required. However, mismatches at the 5' end of the gRNA are tolerated for cleavage. This information is important for us to design the optimized gRNAs to avoid off-target effects.

Multiple approaches were developed to evaluate the Cas9-mediated off-target effects. First, multiple similar sequences in genome were identified by BLAST and were tested by T7E1 or Surveyor assay. This approach is fast and simple, however, it may not reveal off-target effects on other sites and may not be sensitive enough. In silico prediction of target sites and testing them by deep sequencing are emerging to be an accepted method. An unbiased whole-genome sequencing

would be ideal. However, it might be costly and time consuming and therefore, unlikely to be widely used for regular analysis.

In addition, several new strategies were recently developed to improve the specificity or minimize off-target modification of the CRISPR/Cas9 system, including paired Cas9 nickases (Mali et al., 2013a; Ran et al., 2013; Shen et al., 2014), truncated guide RNA (Fu et al., 2014) and titration of dosage for Cas9 and guide RNA (Hsu et al., 2013).

4.2 Prediction of off-target sites.

We tested four different mouse groups for possible off-target effects of CRISPR/Cas9-mediated genome editing: (A) *mdx* mice without treatment (termed *mdx*), (B) CRISPR/Cas9-edited *mdx* mice (termed *mdx*+Cas9), (C) Wild-type control mice (C57BL6/C3H) without treatment (termed WT) and (D) CRISPR/Cas9-edited wild-type mice (termed WT+Cas9) (**Figure 4.1A**). Sequences of the target site (*Dmd* exon 23) and a total of 32 potential off-target (OT) sites in the mouse genome were predicted by CRISPR design tool (<http://crispr.mit.edu/>) and are listed in **Table 4.1**. Ten of the 32 sites, termed OT-01 through OT-10 represent the genome-wide top-ten hits. Twenty-two of the 32, termed OTE-01 through OTE-22 are located within exons.

4.3 Deep sequencing

Deep sequencing of PCR products corresponding to *Dmd* exon 23 revealed high ratios of HDR and NHEJ-mediated genetic modification in groups B and D but not in control groups A and C (**Figure 4.1A and Table 4.3**). There was no difference in the frequency of indel mutations in

the 32 potential off-target regions among the different groups (**Figure 4.1 B and C, Table 4.4**). These results are also consistent with recent genome-wide studies showing that DNA cleavage by Cas9 is not promiscuous (Duan et al., 2014 ; Kuscu et al., 2014; Wu et al., 2014). Thus, off-target effects may be less of a concern in vivo than previously observed in vitro (Fu et al., 2013; Pattanayak et al., 2013).

4.4 Materials and Methods

4.4.1 Sample preparation

Off-target loci were amplified by PCR using primers listed in **table S1** for (A) *mdx* (B) *mdx*+Cas9 (C) WT and (D) WT+Cas9. PCR products were purified by MinElute PCR purification kit (QIAGEN), adjusted to the same concentration (10 ng/ μ L), and equal volumes (5 μ L) were combined for each group. Library preparation was performed according to the manufacturer's instructions (KAPA Library Preparation Kits with standard PCR library amplification module, Kapa Biosystems).

4.4.2 Deep sequencing of off-target sites.

Sequencing was performed on the Hiseq 2500 from Illumina and was run using Rapid Mode 150PE chemistry. Sequencing reads were mapped using BWA (<http://bio-bwa.sourceforge.net/>). Reads with mapping quality greater than 30 were retained for variant discovery. The mean read depth across all regions and all samples was 2570-fold. The variants were called using SAMtools (<http://samtools.sourceforge.net/>) plus custom scripts. In each region, insertion and deletion of 3 base pairs or longer were counted in a 50-bp window centered on the Cas9 potential cleavage sites.

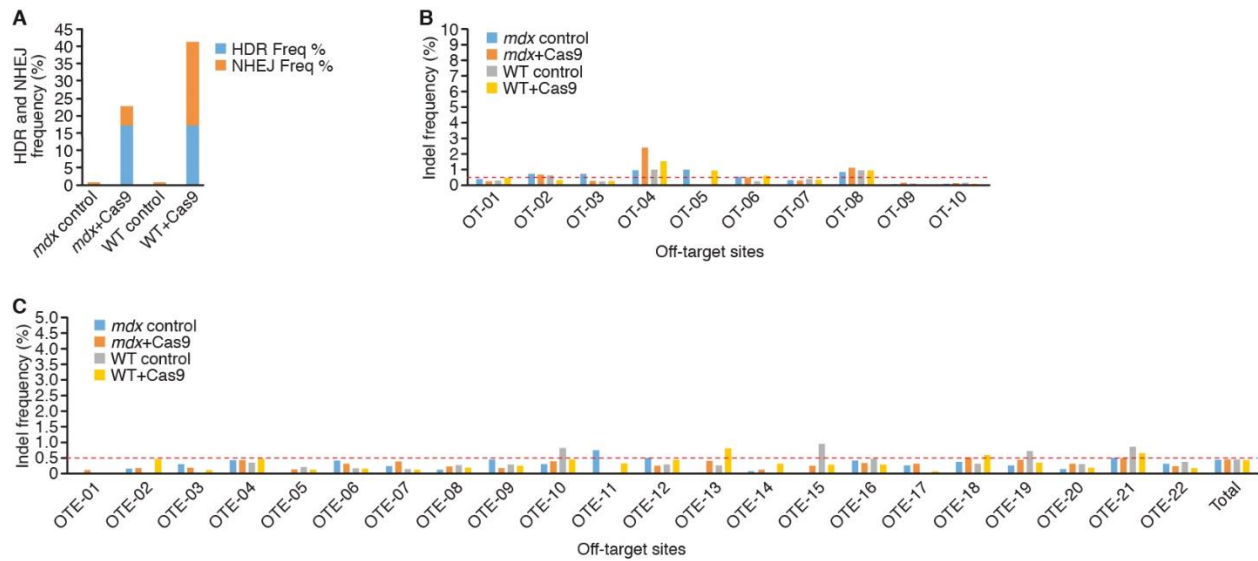


Figure 4.1. Deep sequencing analysis of target site (*Dmd*) and 32 theoretical off-target sites.

(A) Frequency of HDR- and NHEJ-mediated gene correction at target site (*Dmd*) from deep sequencing of DNA from four groups of mice: *mdx*, *mdx*+Cas9, WT and WT+Cas9.

(B) Frequency of NHEJ-mediated indels at genome-wide “top ten” theoretical off-target sites (OT-01 to OT-10) (Table 4.1) from deep sequencing results of DNA from the four groups of mice.

(C) Frequency of NHEJ-mediated indels at twenty-two theoretical off-target sites within exons (OTE-01 to OTE-22) (Table 4.1) from deep sequencing of DNA from the four groups of mice.

Table 4.1. Sequences of the target site (*Dmd* exon 23) and 32 potential off-target (OT) sites in the mouse genome.

#	Target(20nt)-PAM(3nt)	locus (mm10)	score	mismatches	UCSC gene
DMD	TCTTTGAAAGAGCAACAAAATGG	chrX:83803318-83803340	37		
OT-01	TTTTTCAAAGAGCAACAATAAGG	chr16:53976196-53976218	5.5	2MMs [2:19]	
OT-02	TTTTTCAAAGATCAACAAAATAG	chr16:58084165-58084187	4.2	2MMs [2:12]	
OT-03	TCTGTGAAAGAGTAACAAAATGG	chr2:26068637-26068659	3.1	2MMs [4:13]	
OT-04	TCATTGAAAGAGCAACACAAAGG	chr17:85542328-85542350	2.6	2MMs [3:18]	
OT-05	TCTGAGAAATAGCAACAAAAGG	chr5:28127468-28127490	2.3	3MMs [4:5:10]	
OT-06	TCTTTTAAAGAGCAACAATAAGG	chr2:44769953-44769975	2.1	2MMs [6:19]	
OT-07	TCTTTGAAATAGGAACAAAACAG	chr14:93068307-93068329	2	2MMs [10:13]	
OT-08	GCTGTGAAAGAGCAACAAACAAG	chr9:95136798-95136820	1.5	3MMs [1:4:20]	
OT-09	TATTTAAAAAAGCAACAAAAGG	chrX:45387898-45387920	1.5	3MMs [2:6:10]	
OT-10	TCTTTGAAAGTCCAACAAAAGG	chr5:38571962-38571984	1.4	2MMs [11:12]	
OTE-01	ACTTTGAAAAAGCAACACAAAGG	chrX:169303124-169303146	0.6	3MMs [1:10:18]	NM_178754
OTE-02	TCTTTGAGAGAACAACAAACAGG	chr6:78381061-78381083	0.6	3MMs [8:12:20]	NM_011259
OTE-03	TCTTTGACAGAGAAACAAACAGG	chr16:10960046-10960068	0.5	3MMs [8:13:20]	NM_019980
OTE-04	ATTTTCAATGAGCAACAAAATGG	chr6:129053832-129053854	0.5	4MMs [1:2:6:9]	NR_024262
OTE-05	AATTTAAAAGAGAAACAAAATAG	chr2:118748097-118748119	0.4	4MMs [1:2:6:13]	NR_030716
OTE-06	TGTTTGAACCAGCAACAATGAG	chr1:90830366-90830388	0.4	4MMs [2:9:10:20]	NM_001243008
OTE-07	TTTTTCAAAGAGAAGCAAAAATAG	chr3:28668648-28668670	0.3	3MMs [2:13:15]	NM_026910
OTE-08	CCTTTGAGAGAACAACAAACAGG	chr8:109728362-109728384	0.3	4MMs [1:8:12:20]	NM_001080930
OTE-09	TTTATGAAACAGCAACAGAAAGG	chr2:76705331-76705353	0.3	4MMs [2:4:10:18]	NM_028004
OTE-10	TGTTAGAATGAGCAACAATCAG	chr2:126908236-126908258	0.3	4MMs [2:5:9:19]	NM_023220
OTE-11	TATTTAAAATAGGAACAAAAGG	chr9:88581220-88581242	0.3	4MMs [2:6:10:13]	NM_001034906
OTE-12	TCATAGAAAGAGCAACCAATCAG	chr4:32723618-32723640	0.3	4MMs [3:5:17:20]	NM_001081392
OTE-13	TCTTGGAAAGAGGAAAAAAGG	chr19:26696234-26696256	0.2	3MMs [5:13:16]	NM_011416
OTE-14	TGTTTGTAAAGGAAACAAAAGG	chr16:10170610-10170632	0.2	4MMs [2:7:11:13]	NM_026594
OTE-15	TCTTTCAAGCAGAAACAAAACAG	chr1:139447127-139447149	0.2	4MMs [6:9:10:13]	NM_172643
OTE-16	TCTGTGAAACAGTAACTAAACGG	chr5:134295459-134295481	0.2	4MMs [4:10:13:17]	NM_001080748
OTE-17	TCTTTGAAAGAGTATCTAAAAGG	chr2:79672854-79672876	0.1	3MMs [13:15:17]	NM_080558
OTE-18	TATATGAAAGAGCCACAAGATGG	chr10:20988803-20988825	0.1	4MMs [2:4:14:19]	NM_026203
OTE-19	TATTAGAAAGAGAAAGAAAAGG	chr1:161837651-161837673	0.1	4MMs [2:5:13:16]	NM_172645
OTE-20	TCACTGAAAGAGCAAGAAAAGG	chr16:48977882-48977904	0.1	4MMs [3:4:16:17]	NM_001110017
OTE-21	TCTCTGAAGGAACAACAACAAGG	chr7:45425042-45425064	0.1	4MMs [4:9:12:19]	NM_011304
OTE-22	TCTTTACAAGATCATCAAAAAGG	chr11:60875710-60875732	0.1	4MMs [6:7:12:15]	NM_001168507

Table 4.2 Primers for OT analysis

DMD232_f	cttctattttaattttgaggctctgc
DMD232_r	cctgaaatttttcgaagtttattcat
DS-OT-01_f	tatgccacttcttcaaagagatgat
DS-OT-01_r	aacaagcaaacaattcaaaggatag
DS-OT-02_f	aagaagatatggcattgctggta
DS-OT-02_r	tctggaacaaaaaggcaatg
DS-OT-03_f	taagagttctgacatgatttccaca
DS-OT-03_r	tggaacactactctctacactgtgc
DS-OT-04_f	ctatgagtttaccaccctaattgtgc
DS-OT-04_r	cttatgcttgttcaggcaaatacc
DS-OT-05_f	ttttgagttgtggttcattttctgag
DS-OT-05_r	taggagtacagctgcttcttcagac
DS-OT-06_f	gaaaaacaaaattactgaggcatgt
DS-OT-06_r	cctccaagttcttatcttgtttgaa
DS-OT-07_f	agtgattttctgatgacccaaatta
DS-OT-07_r	tgtttttaatggctagggtgctaatac
DS-OT-08_f	tttcttgagctgtagtggtactg
DS-OT-08_r	ggaatagagtgagcattggtctgat
DS-OT-09_f	tgtcacagttgcaattcttagtggt
DS-OT-09_r	cttagaaaaacaaggttctgacaa
DS-OT-10_f	caataaggacaagtgaaggctaaaa
DS-OT-10_r	aggctccacacatatcactcttc
DS-OTE-01_f	agatctgggagcttctatcaactg
DS-OTE-01_r	gggtagaagtgaatcaataagtgga
DS-OTE-02_f	gaacacttctttgcttctcatcact
DS-OTE-02_r	gctgagactactgtagccctttaga
DS-OTE-03_f	tagtttttcacattcagtcagctt
DS-OTE-03_r	gctttcaaaactacaccaaactac
DS-OTE-04_f	ctttaaaatacaagcctccagttcc
DS-OTE-04_r	tatttgtttctcaaatttccagacc
DS-OTE-05_f	attttctagaggtggtctcacacac
DS-OTE-05_r	gaaaagtggatagacagtttcagga
DS-OTE-06_f	aacctaaaagaaaggacaaggagaa
DS-OTE-06_r	acatgactcggtataataaaccttgag
DS-OTE-07_f	ttgtaaaagttccaactcccagtag
DS-OTE-07_r	tttaaaatctatttcccagagagg
DS-OTE-08_f	tgtccatttttaacctgtgttctg
DS-OTE-08_r	ccctaactcagtttctcttgttctg
DS-OTE-09_f	atctgtgttttcaatgtggaatctt
DS-OTE-09_r	agaaagcgaataggatttcttgttt

DS-O TE-10_f	tcgaatc t t t c t a c a a t a t g c a a t c a
DS-O TE-10_r	g t g g g a a a t g t t t c a a g t a t c a c a t
DS-O TE-11_f	g c a a a a t a c a a c t t c t a a g c a a a c c
DS-O TE-11_r	c c a g a c c a g a g g t a g a g t g t t t c t a
DS-O TE-12_f	c a g g a g t c a g c c t c t t a c t t t a c a a
DS-O TE-12_r	g c t a g a t g a c a a a g c c a c t t a a c t c
DS-O TE-13_f	g c t a c a g a a a a g a g g c t a g g a a a g t
DS-O TE-13_r	g c t t t g a a g a t g c c c t a g a a a t a c t
DS-O TE-14_f	t a a t a c a t a a g g g g a c a t c a c g a g t
DS-O TE-14_r	g a t c t t t g t a g t g g t t t t t c t c c t g
DS-O TE-15_f	t t a a g c g g a a a g a t a a g c t g a a g t a
DS-O TE-15_r	g g a c c a a t g t t a c t g g a a c a c a t a c
DS-O TE-16_f	c t t c t a c a t t c a c c t c c c t g t g t t
DS-O TE-16_r	c c c a g c a t c t a a g a a g g a g t a a t a
DS-O TE-17_f	a a a t t t t t a g t c a a a a g t g c t t g g a
DS-O TE-17_r	c a a t a a c c t t t c a g a c t t c a t t g g
DS-O TE-18_f	t a t g a t t t c c a g g g t a a g t c c a c t a
DS-O TE-18_r	g c a c t t t t g c t a a c a t c t a a a t t c c
DS-O TE-19_f	a a a g t a t a t c t g a g a a t g c c a c t g c
DS-O TE-19_r	g t a g c t g t a g g a a t g t c t g t c c t g t
DS-O TE-20_f	t g t a a t a a a a t g a g a a t t t g c a c c a
DS-O TE-20_r	a a t g a a g c c a a g g t a c a t a c a a a g a
DS-O TE-21_f	c a t g a a g a t a c a g a a a c a t c c c a g t
DS-O TE-21_r	g g a g t g g c a c c c t c c t t a c
DS-O TE-22_f	a t a c c c c a a g c c a t a c t t g t a t c a t
DS-O TE-22_r	c a c t t a t c c a t c t a g g a a a g c a g a g

Table 4.3. Deep sequencing results of PCR products from the *Dmd* target site.

Target Site	Group	HDR Reads	Del. Reads	In. Reads	Total Reads	NHEJ (indel) Freq %	HDR Freq %	Total Freq %
<i>Dmd</i>	A: <i>mdx</i> control	0	45	6	6623	0.77	0	0.77
	B: <i>mdx</i>+Cas9	1363	51	384	7975	5.45	17.09	22.54
	C: WT control	0	27	4	4663	0.66	0	0.66
	D: WT+Cas9	1211	1665	11	7024	23.86	17.24	41.10

Table 4.4. Deep sequencing results of PCR products from 32 potential off-target regions.

Site	Chr.	GroupA: <i>mdx</i> control				GroupB: <i>mdx</i> +Cas9				GroupC: WT control				GroupD: WT+Cas9			
		Del. Reads	In. Reads	Total Reads	Indel Freq %	Del. Reads	In. Reads	Total Reads	Indel Freq %	Del. Reads	In. Reads	Total Reads	Indel Freq %	Del. Reads	In. Reads	Total Reads	Indel Freq %
OT-01	16	6	1	1781	0.39	7	0	2811	0.25	3	1	1358	0.29	8	0	1732	0.46
OT-02	16	12	1	1797	0.72	16	0	2351	0.68	6	0	946	0.63	4	0	1243	0.32
OT-03	2	15	1	2196	0.73	11	0	4004	0.27	4	0	1729	0.23	4	1	1968	0.25
OT-04	17	27	16	4511	0.95	63	36	4101	2.41	30	16	4609	1.00	42	20	4074	1.52
OT-05	5	4	2	598	1.00	0	0	197	0.00	0	0	332	0.00	5	1	645	0.93
OT-06	2	13	2	2741	0.55	24	3	5516	0.49	6	0	2431	0.25	18	1	3191	0.60
OT-07	14	5	0	1527	0.33	7	2	3116	0.29	6	0	1504	0.40	4	1	1444	0.35
OT-08	9	55	12	8009	0.84	63	26	8018	1.11	70	2	7689	0.94	71	4	7925	0.95
OT-09	X	1	0	2075	0.05	3	1	2521	0.16	2	0	1911	0.10	0	0	2870	0.00
OT-10	5	2	0	2109	0.09	4	1	3606	0.14	2	1	1905	0.16	2	1	3129	0.10
OTE-01	X	0	0	653	0.00	2	0	1727	0.12	0	0	569	0.00	0	0	988	0.00
OTE-02	6	1	0	626	0.16	2	1	1669	0.18	0	0	490	0.00	4	0	873	0.46
OTE-03	16	5	0	1657	0.30	7	1	4304	0.19	0	0	1202	0.00	2	0	1733	0.12
OTE-04	6	13	4	3941	0.43	25	3	6546	0.43	10	0	2825	0.35	28	3	6524	0.48
OTE-05	2	0	0	563	0.00	1	0	774	0.13	1	0	480	0.21	1	0	860	0.12
OTE-06	1	10	0	2423	0.41	18	0	5763	0.31	7	0	4176	0.17	9	1	6277	0.16
OTE-07	3	2	0	854	0.23	5	0	1293	0.39	1	0	682	0.15	1	0	809	0.12
OTE-08	8	7	1	6815	0.12	13	5	8016	0.22	9	4	4835	0.27	12	1	6962	0.19
OTE-09	2	13	1	3080	0.45	8	0	4542	0.18	2	1	1017	0.29	7	1	3310	0.24
OTE-10	2	4	0	1323	0.30	7	0	1766	0.40	8	0	976	0.82	8	0	1760	0.45
OTE-11	9	3	0	402	0.75	0	0	350	0.00	0	0	428	0.00	2	0	619	0.32
OTE-12	4	9	2	2143	0.51	8	0	3246	0.25	4	0	1395	0.29	10	1	2496	0.44
OTE-13	19	0	0	1238	0.00	10	2	2930	0.41	4	0	1560	0.26	10	0	1240	0.81
OTE-14	16	1	0	1288	0.08	3	0	2515	0.12	0	0	693	0.00	2	1	944	0.32
OTE-15	1	0	0	607	0.00	4	0	1585	0.25	5	0	522	0.96	3	0	1048	0.29
OTE-16	5	11	1	2862	0.42	10	2	3560	0.34	18	2	4193	0.48	16	1	5952	0.29
OTE-17	2	3	0	1159	0.26	7	0	2216	0.32	0	0	1120	0.00	1	0	1533	0.07
OTE-18	10	4	0	1080	0.37	10	0	1933	0.52	2	0	639	0.31	6	0	1025	0.59
OTE-19	1	3	0	1173	0.26	13	0	2980	0.44	8	0	1101	0.73	5	1	1734	0.35
OTE-20	16	1	0	668	0.15	3	1	1274	0.31	2	0	669	0.30	2	0	1074	0.19
OTE-21	7	8	3	2157	0.51	22	2	4873	0.49	21	0	2425	0.87	20	1	3226	0.65
OTE-22	11	9	0	2828	0.32	9	2	4624	0.24	9	0	2423	0.37	5	1	3257	0.18
Total		247	47	66884	0.44	385	88	104727	0.45	240	27	58834	0.45	312	41	82465	0.43

Chapter 5 Histological and functional analysis of corrected *mdx* mice

5.1 Introduction

To evaluate the efficacy of a therapeutic strategy for DMD, standard parameters to measure muscular dystropathology and function in *mdx* mice were developed (Grounds et al., 2008).

Immunohistochemical (IHC) analysis is performed on tissues to evaluate the rescue of dystrophin expression in *mdx* mice. Multiple antibodies specific to unique epitopes in different exons of dystrophin has been generated and tested in histological analyses and western blot analysis (Kodippili et al., 2014). These antibodies can be used to map gene deletion at the protein level and diagnosis of various types of muscular dystrophy. In addition to immunological analysis, molecular analysis of DNA and/or mRNA is required for *mdx* mice subjected to gene editing.

Additionally, necrosis, fibrosis and regeneration of muscle are evaluated by histological measurements. Muscular dystropathology in *mdx* mice is typically studied by hematoxylin and eosin (H&E) staining on the transverse sections of various skeletal muscles. At 3 weeks of age when mouse muscle is mature, muscle necrosis can be detected in hind limb muscles. At 8 weeks of age, severe atrophy, inflammation and fibrosis are present in most of the muscle groups in *mdx* mice. Regenerated myofibers have centralized nuclei, which can be used as an indicator of previously damaged/regenerated muscle tissues.

Serum creatine kinase (CK) level is an index of the extent of myofibers leakage and is widely used as a diagnostic marker for muscular dystrophy in human patients. In normal muscle cells, CK is present in a high concentration but serum has low CK levels. During the process of muscle degeneration, the cellular contents leak into the bloodstream and can be detected as a high level. CK level in *mdx* mice have a range of 1,000-20,000U/L, while CK levels in wild type mice are usually less than 500U/L. Decreasing levels of serum CK can be used as an indicator of reduction of myopathy in treated *mdx* mice.

The grip strength test is a standard measurement of muscle strength in mice. It is conducted using a wire mesh grid connected to a horizontally-aligned force meter. Mice are held at the base of their tail and supported ventrally while being moved into a position to grasp a wire grid. Once successfully grasped, ventral support is released and the tail is gently pulled in a horizontal plane until the animal's grip is released from the grid. Peak force (in grams) is captured by the force meter and recorded for later analysis. Forelimb and hindlimb tests are conducted separately, with each being measured 5 times over a 2-3 minute period. The *mdx* mice show significant reduced grip strength at 4 weeks of age in both forelimb and hindlimb compared to wild type mice (C57BL/10ScSnJ). While at 8 weeks, only forelimb grip strength is decrease in the *mdx* mice.

5.2 Immunohistochemical (IHC) analysis

To analyze the effect of CRISPR/Cas9-mediated genomic editing on the development of muscular dystrophy, we performed histological analyses of four different muscle types [quadriceps, soleus (hindlimb muscle), diaphragm (respiratory muscle) and heart muscle] from wild-type mice, *mdx* mice, and three chosen *mdx-C* mice with different percentages of *Dmd* gene correction at 7-9 weeks old age. *mdx* muscle showed histopathologic hallmarks of muscular dystrophy, including variation in fiber diameter, centralized nuclei, degenerating fibers, necrotic fibers, and mineralized fibers, as well as interstitial fibrosis (**Figure 5.1**). Immunohistochemistry showed no dystrophin expression in skeletal muscle or heart of *mdx* mice, while wild-type mice showed dystrophin expression in the subsarcolemmal region of the fibers and the heart (**Figure 5.1**). Although *mdx* mice carry a stop mutation in the *Dmd* gene, we observed 0.2-0.6% revertant fibers, consistent with a previous report (Pigozzo et al., 2013). *mdx-C* mice with 41% of the *mdx* alleles corrected by HDR (termed HDR-41%) or with 83% correction by in-frame NHEJ (termed

NHEJ-83%) showed complete absence of the dystrophic muscle phenotype and restoration of dystrophin expression in the subsarcolemmal region of all myofibers (**Figure 5.1**). Strikingly, correction of only 17% of the mutant *Dmd* alleles (termed HDR-17%) was sufficient to allow dystrophin expression in a majority of myofibers at a level of intensity comparable to that of wild-type mice, and the muscle exhibited fewer histopathologic hallmarks of muscular dystrophy than *mdx* muscle (**Figure 5.4**). The substantially higher percentage (47-60%) of dystrophin-positive fibers associated with only 17% gene correction (**Figure 5.3**) suggests a selective advantage of the corrected skeletal muscle cells.

5.3 Western blot analysis

Western blot analysis showed restored dystrophin protein in skeletal muscle (quadriceps) and heart of *mdx-C* mice to levels consistent with percentages of dystrophin-positive fibers. . The same pattern of bands was observed in samples from wild-type and *mdx-C* mice. (**Figure 5.2**).

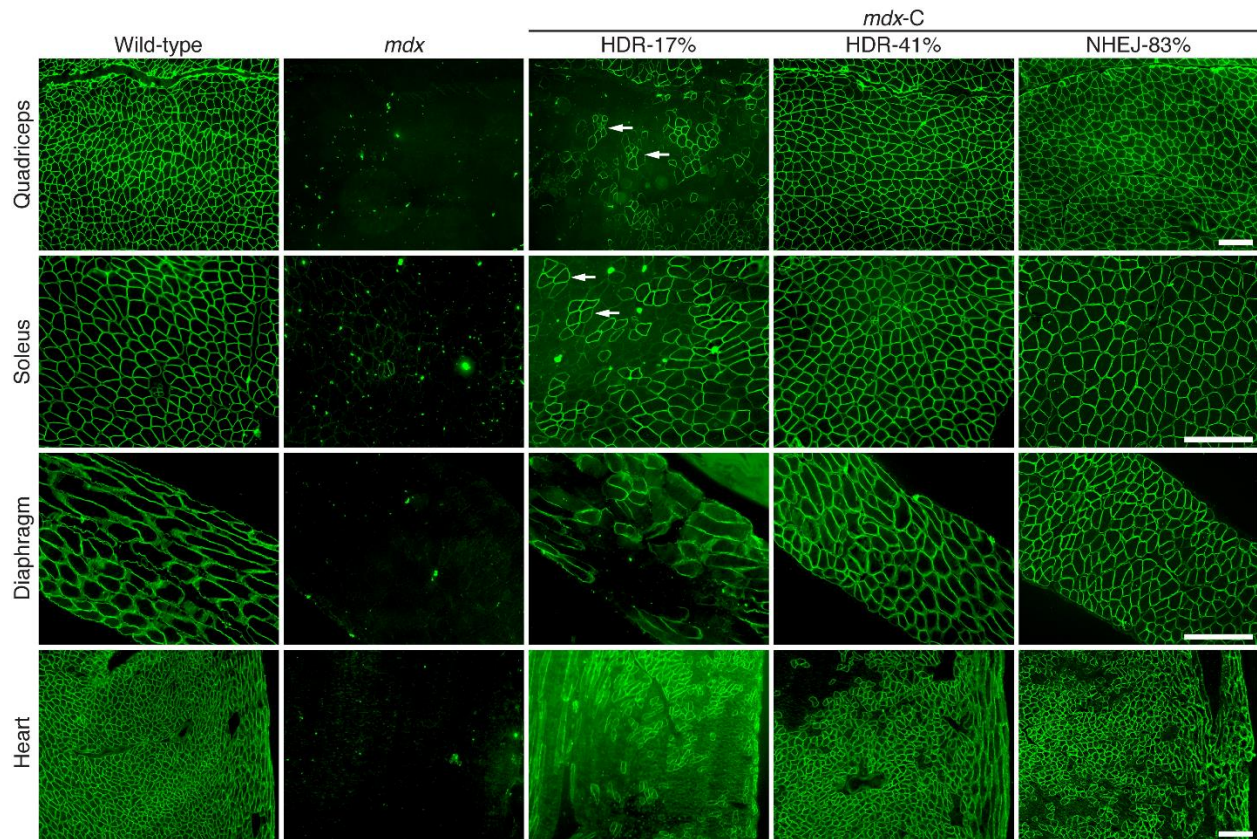


Figure 5.1 Histological analysis of muscles from wild-type, *mdx* and *mdx-C* mice. Immunostaining and histological analysis of muscles from 7-9 week old wild-type, *mdx* and *mdx-C* mice (HDR-17%, HDR-41% or NHEJ-83%). Dystrophin immunofluorescence (green) in wild-type mice is present in all muscles, including quadriceps, soleus, diaphragm and heart and is absent in *mdx* mice, except for a single revertant fiber in skeletal muscle. Skeletal muscle from the HDR-17% mouse has a unique pattern of clusters of dystrophin-positive fibers adjacent to clusters of dystrophin-negative fibers, while HDR-41% or NHEJ-83% *mdx-C* skeletal muscle is composed of dystrophin-positive myofibers only. White arrows indicate the adjacent clusters of dystrophin-positive fibers. Scale bar, 100 microns.

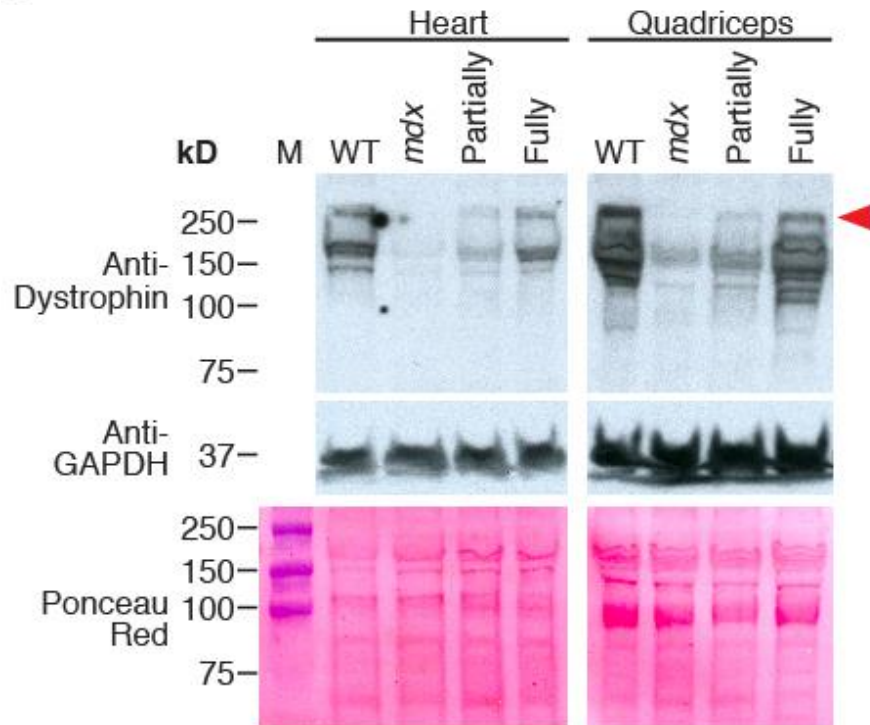


Figure 5.2 Western blot analysis of heart and skeletal muscle (quadriceps) samples from wild-type, *mdx*, and partially corrected (HDR-17%) and fully corrected (HDR-41%) *mdx-C* mice. Red arrowhead (>250kD) indicates the immunoreactive bands of dystrophin. Lower bands (<250kD), which were also absent in *mdx* samples, likely represent proteolytic breakdown of full-length dystrophin protein, natural variants or protein synthesis intermediates. GAPDH is a loading control. PVDF membrane was stained for total protein by 2% Ponceau Red. M denotes size marker lane. kD indicates the protein length of the marker bands.

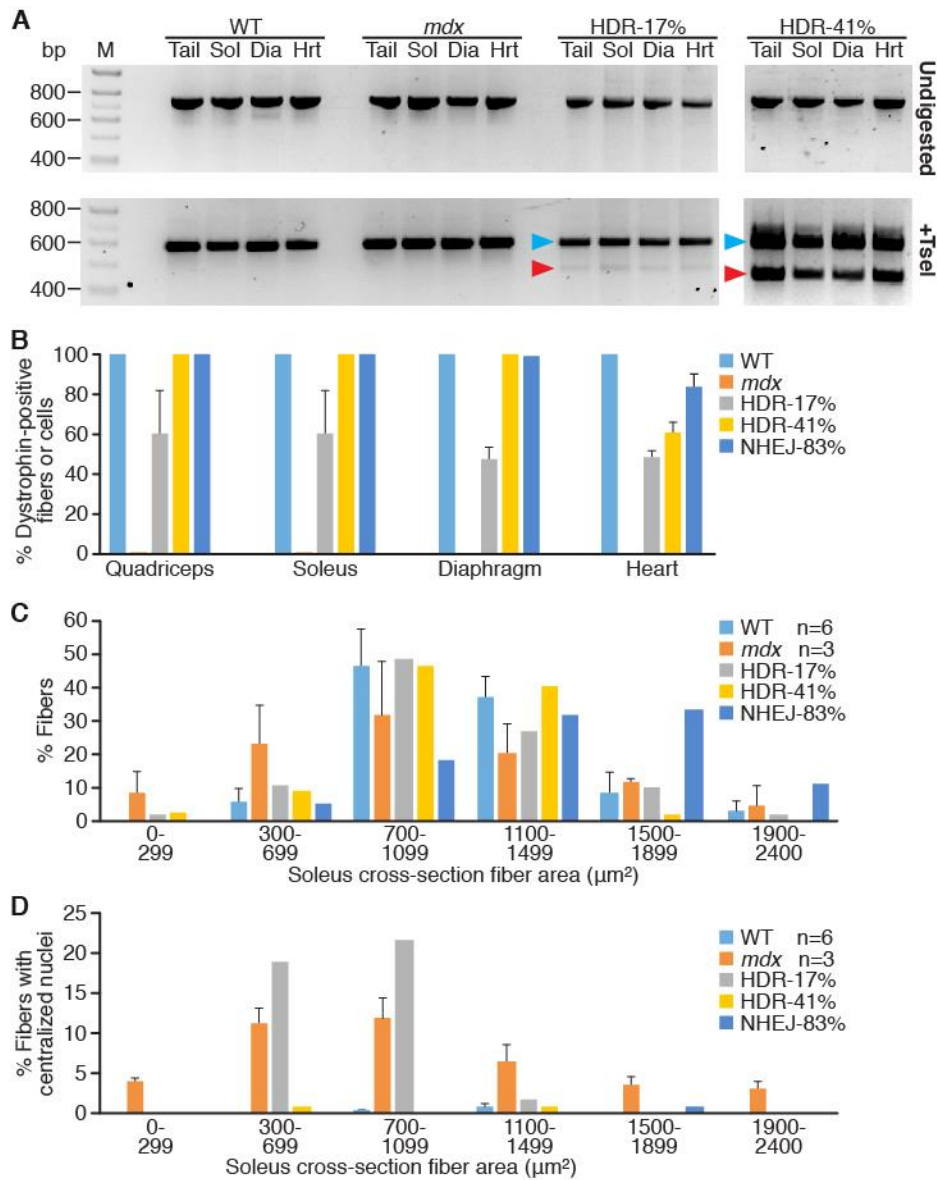


Figure 5.3. RFLP analysis and myofiber measurements of muscle from wild-type, *mdx*, and corrected *mdx-C* mice.

(A) RFLP analysis to quantify the degree of mosaicism of genomic DNA isolated from tail, soleus (Sol), diaphragm (Dia) and heart (Hrt) of wild-type, *mdx*, HDR-17% and HDR-41% mice. PCR was performed using genomic DNA using primers

(Dmd729F and Dmd729R) (upper panel) and digested with TseI (lower panel). DNA products were loaded on a 2% agarose gel. The red arrowhead marks the DNA band indicating HDR-mediated correction, generated by TseI digestion. The blue arrowhead marks the DNA band of the uncorrected *mdx* allele. M denotes size marker lane. bp indicates the base pair length of the marker bands.

(B) Quantification of dystrophin-positive cells in quadriceps, soleus, diaphragm and heart. n= 6 for WT; n=3 for *mdx*. Error bars show standard deviation based on data from multiple muscle sections.

(C) Measurement of the distribution of the cross-sectional areas of myofibers from the soleus of wild-type mice showed uniformly sized fibers with 90% of the fibers ranging from 700-1499 μm^2 . In contrast, myofibers from *mdx* mice were heterogeneous in size, ranging between 300-1899 μm^2 . The size distribution of the myofibers from HDR-41% muscle was strikingly similar to that of wild-type mice. n= 6 for WT; n=3 for *mdx*. Error bars show standard deviation based on data from multiple muscle sections.

(D) Distribution of soleus myofibers with centralized nucleus. The percentage of regenerated myofibers of muscle from HDR-17% ranged from 700-1099 μm^2 , which was higher than the percentage of fibers from the *mdx* muscle.

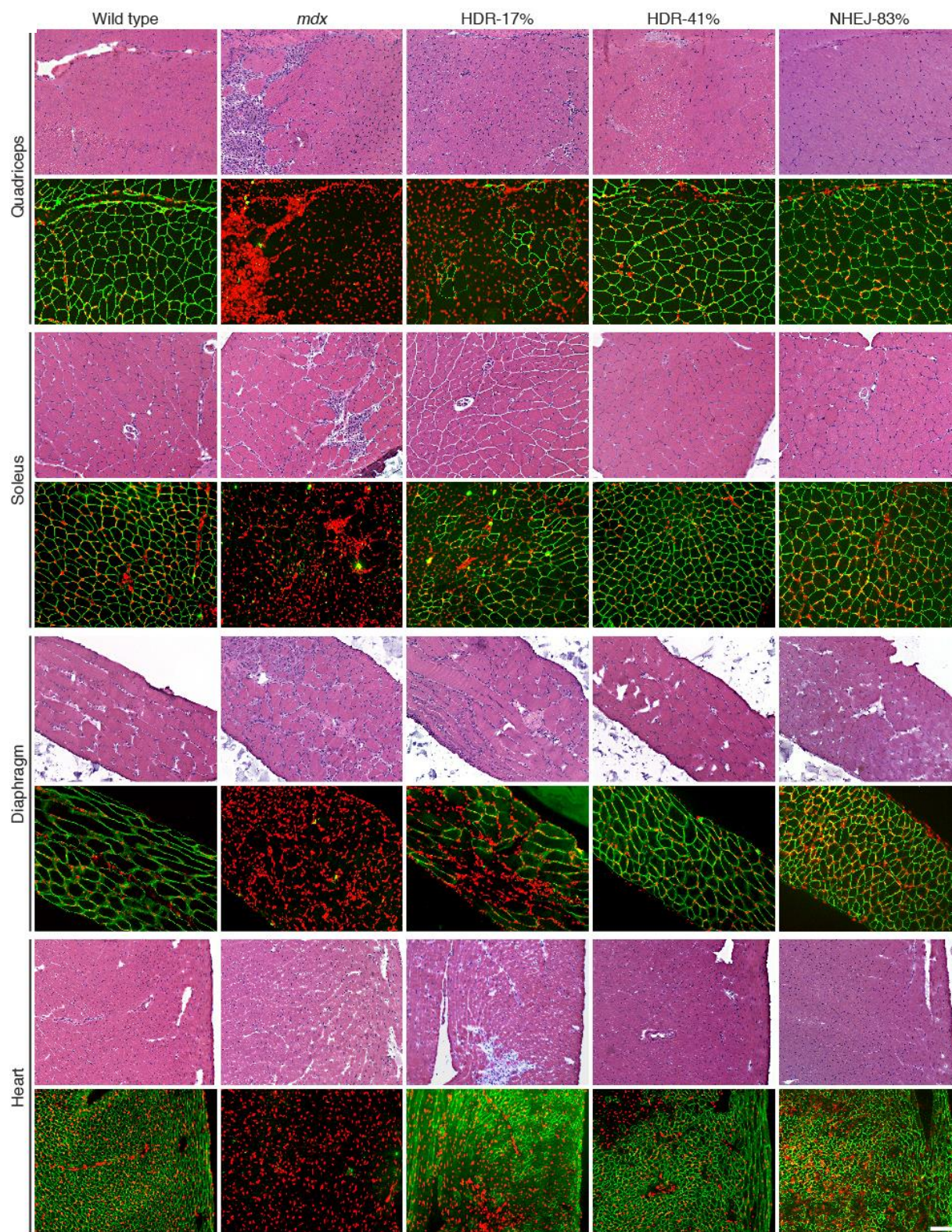


Figure 5.4 Hematoxylin and eosin (H&E) and immunostaining of muscles from 7-9 week old wild-type, *mdx*, and *mdx-C* mice (HDR-17%, HDR-41% and NHEJ-83% corrected allele; as seen in **Fig. 2**). Immunofluorescence (green) detects dystrophin. Nuclei are labeled by propidium iodide (red). Scale bar, 100 microns.

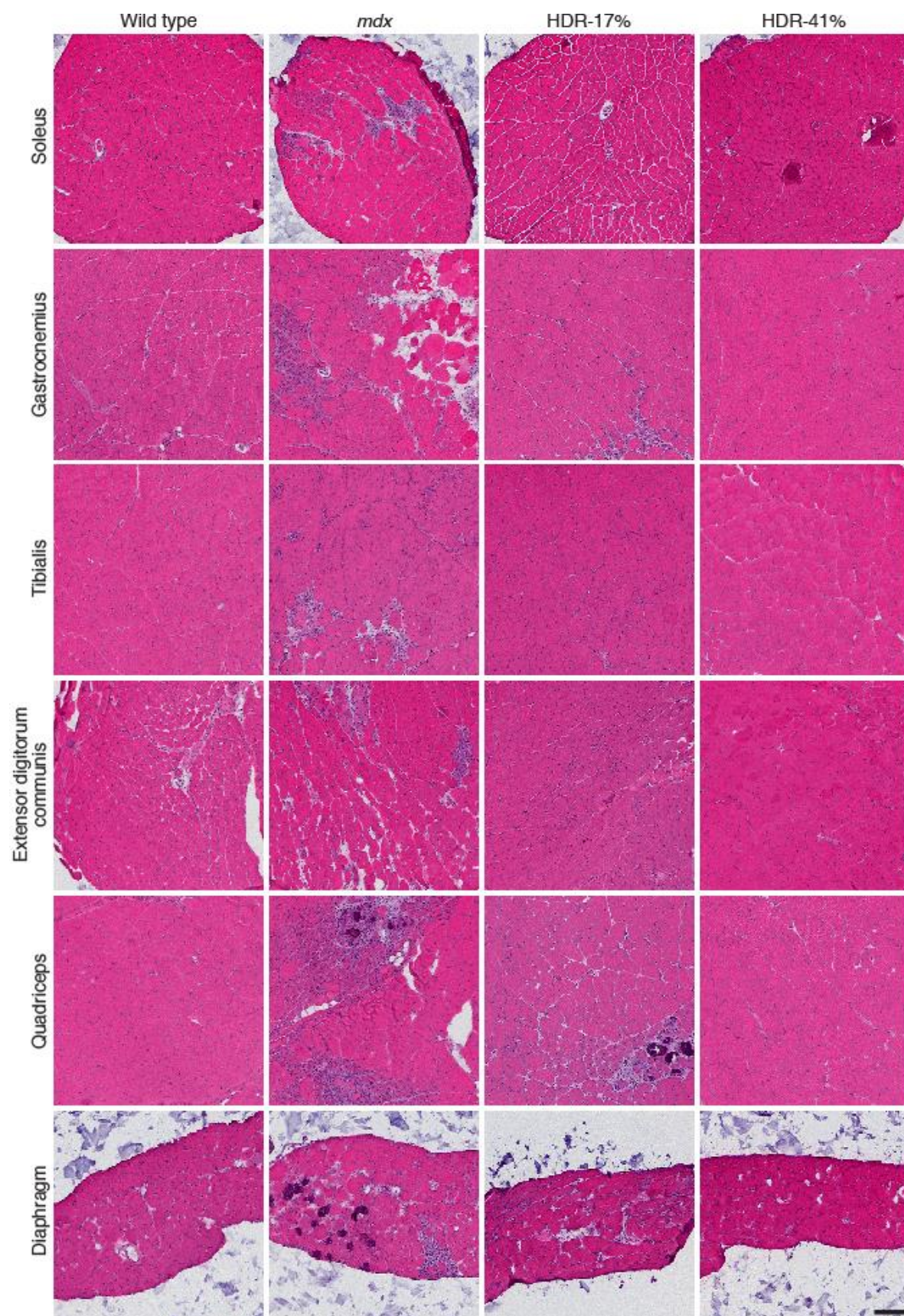


Figure 5.5. Histology of muscles showing decrease in fibrosis and necrosis by CRISPR/Cas9-mediated genomic editing of *Dmd* allele.

Hematoxylin and eosin (H&E) stained transverse cryosections of whole soleus, gastrocnemius, tibialis-anterior, extensor-digitorum-communis, quadriceps, and diaphragm from 7-9 week old wild-type, *mdx*, HDR-17% and HDR-41% and Scale bar, 125 microns.

5.4 Functional assay

Serum creatine kinase (CK), a diagnostic marker for muscular dystrophy that reflects muscle leakage, was measured in wild-type, *mdx* and *mdx-C* mice. Consistent with the histological results, serum CK levels of the *mdx-C* mice were substantially decreased compared to *mdx* mice and were inversely proportional to the percentage of genomic correction (**Table 5.1**). Wild-type, *mdx*, and *mdx-C* mice were also subjected to grip strength testing to measure muscle performance, and the *mdx-C* mice showed enhanced muscle performance compared to *mdx* mice (**Table 5.1**).

Table 5.1. Serum creatine kinase (CK) levels and forelimb grip strength of wild-type, *mdx* and *mdx-C* mice.

Litter	mouse #	Percent of Correction	Sex	CK(U/L)	Forelimb Grip Strength (grams of force)					
					Trial1	Trial2	Trial3	Trial4	Trial5	Avg. \pm SD
#1	WT	-	M	318	170	163	140	132	169	154.8 \pm 17.5
	<i>mdx</i> -04	0	M	6,366	64	56	52	59	57	57.6 \pm 4.3
	<i>mdx</i> -06	0	M	7,118	102	123	109	79	97	102.0 \pm 16.1
	<i>mdx-C</i>1	HDR-41%	M	350	141	150	154	143	133	144.2\pm8.1
#2	WT	-	F	449	128	116	109	102	103	111.6 \pm 10.7
	<i>mdx</i> -20	0	F	30,996	107	105	92	78	61	88.6 \pm 19.3
	<i>mdx</i> -10	0	F	38,715	84	64	67	62	53	66.0 \pm 11.3
	<i>mdx-C</i>3	HDR-17%	F	4,290	123	126	101	107	102	111.8\pm11.8
#25	<i>mdx</i> -02	0	M	14,059	54	64	47	41	52	51.6 \pm 12.1
	<i>mdx</i> -03	0	M	4,789	129	120	116	104	92	112.2 \pm 35.6
	<i>mdx</i> -05	0	M	11,841	91	94	54	64	54	71.4 \pm 24.0
	<i>mdx-N</i>1	NHEJ-83%	M	240	145	154	147	138	133	143.4\pm44.8
	<i>mdx</i> -01	0	F	7,241	108	95	103	105	85	99.2 \pm 30.5
	<i>mdx</i> -04	0	F	5,730	100	112	103	114	100	105.8 \pm 32.3
	<i>mdx</i> -07	0	F	6,987	74	73	73	73	70	72.6 \pm 19.6

5.5 Materials and Methods

5.5.1 Histological analysis of muscles.

Skeletal muscle from wild-type, *mdx*, and corrected *mdx-C* mice were individually dissected and cryoembedded in a 1:2 volume mixture of Gum Tragacanth powder (Sigma-Aldrich) to Tissue Freezing Medium (TFM) (Triangle Bioscience). Hearts were cryoembedded in TFM. All embeds were snap frozen in isopentane heat extractant supercooled to -155 °C. Resulting blocks were stored overnight at -80 °C prior to sectioning. Eight-micron transverse sections of skeletal muscle, and frontal sections of heart were prepared on a Leica CM3050 cryostat and air-dried prior to same day staining. H&E staining was performed according to established staining protocols and dystrophin immunohistochemistry was performed using MANDYS8 monoclonal antisera (Sigma-Aldrich) with modifications to manufacturer's instructions. In brief, cryostat sections were thawed and rehydrated/delipidated in 1% triton/phosphate-buffered-saline, pH 7.4 (PBS). Following delipidation, sections were washed free of Triton, incubated with mouse IgG blocking reagent (M.O.M. Kit, Vector Laboratories), washed, and sequentially equilibrated with MOM protein concentrate/PBS, and MANDYS8 diluted 1:1800 in MOM protein concentrate/PBS. Following overnight primary antibody incubation at 4 °C, sections were washed, incubated with MOM biotinylated anti-mouse IgG, washed, and detection completed with incubation of Vector fluorescein-avidin DCS. Nuclei were counterstained with propidium iodide (Molecular Probes) prior to cover slipping with Vectashield.

5.5.2 Imaging and analysis.

Specimens were reviewed with a Zeiss Axioplan 2iE upright photomicroscope equipped with epifluorescence illumination, CRI color wheel, and Zeiss Axiocam monochromatic CCD camera. OpenLab 4.0 acquisition and control software (Perkin-Elmer) was used to capture 10x and 20x objective magnification fields, and further used to apply indexed pseudocoloring and merge image overlays. Images were peak levels-adjusted with Adobe Photoshop CS2 and saved for image analysis. ImageJ 1.47 was used to apply stereologic morphometric randomization grid overlays and the software's counting functions used to mark and score approximately 500 aggregate myofibers (from a minimum of three interval-sections) for dystrophin positive and negative immunostaining from each muscle group. H&E stained sections of soleus muscle for each genotype were further analyzed with ImageJ 1.47 for size and characteristic. In brief, sarcolemmal boundaries of 115+ stereologically randomized myofibers were manually delineated, their cross sectional area calculated, and central-nuclear phenotype recorded.

5.5.3 Western blot analysis.

Muscles were dissected and rapidly frozen in liquid nitrogen. Protein extraction and western blot analysis were performed as described (Kodippili et al., 2014; Nicholson et al., 1989) with modification. Samples were homogenized with a homogenizer (POLYTRON System PT 1200 E) for 2 X 20 seconds in 400 μ L sample buffer containing 10%SDS, 62.5 mM Tris, 1mM EDTA and protease inhibitor (Roche). Protein concentration was measured using the BCA Protein Assay Kit (Pierce). Fifty micrograms of protein from each muscle sample was loaded onto a gradient SDS-PAGE (Bio-Rad). The gel was run at 100V for 2.5 hours. Separated proteins were transferred to a PVDF membrane at 35V overnight in a cold room (4°C). The PVDF membrane

was stained for total protein using 2% Ponceau Red and then blocked for one hour with 5% w/v nonfat dry milk, 1X TBS, 0.1% Tween-20 (TBST) at 25 °C with gentle shaking. The blocked membrane was incubated with a mouse anti-dystrophin monoclonal antibody (MANDYS8, Sigma-Aldrich, 1: 1,000 dilution in 5% milk/TBST) overnight at 4 °C and then washed in TBST. The blot was then incubated with horseradish peroxidase conjugated goat anti-mouse IgG secondary antibody (Bio-Rad, 1:10,000 dilution) for one hour at 25 °C. After washing with TBST, the blot was exposed to Western Blotting Luminol Reagent (Santa Cruz Biotech) for 1 min to detect signal. Protein loading was monitored by anti-GAPDH antibody (Millipore, 1:10,000 dilution).

5.5.4 Serum creatine kinase (CK) measurement.

Blood was collected from the submandibular vein and serum CK level was measured by VITROS Chemistry Products CK Slides to quantitatively measure CK activity using VITROS 250 Chemistry System.

5.5.5 Grip strength test.

Muscle strength was assessed by a grip strength behavior task performed by the Neuro-Models Core Facility at UT Southwestern Medical Center. The mouse was removed from the cage, weighed and lifted by the tail causing the forelimbs to grasp the pull-bar assembly connected to the grip strength meter (Columbus Instruments). The mouse was drawn along a straight line leading away from the sensor until the grip is broken and the peak amount of force in grams was recorded. This was repeated 5 times.

Chapter 6 A model for rescue of muscular dystrophy by CRISPR/Cas9

6.1 Introduction

More than half a century ago, Alexander Mauro identified a type of rare mononuclear cell localized between the plasma membrane of muscle fiber and basement membrane (Mauro, 1961). These cells, termed satellite cells, were found to be the key contributor to adult skeletal muscle regeneration. The majority of satellite cells are present in a quiescent state in normal conditions. In response to injury, exercise or other mechanic strain, the satellite cells become activated and re-enter the cell cycle. The differentiated cells fuse with each other or with existing myofibers to generate new muscle tissue (**Figure 6.1**).

With the ability to regenerate the injured muscle tissue and the ability of self-renewal, satellite cells are considered to be the ideal candidates for cell-based transplantation and have a great therapeutic value to treat muscular diseases, such as DMD. Although *mdx* mice or DMD patients have satellite cells, these cells also contain the mutation in the dystrophin gene which cannot rescue the disease. Normal satellite cells or myoblast cells with a functional dystrophin gene are required for the transplantation. Despite the promising results in the mouse model, this approach encounters the following therapeutic challenges: 1) in vitro expansion of satellite cells from healthy donors are required, however, these cells lose proliferative potential and regenerative capacity during cell culture. Satellite cell self-renewal and differentiation are regulated by their niches in vivo, hence isolated satellite cells begin to exit the quiescent state 2) Implanted cells have a poor migration capacity. 3) Immunosuppressant drugs have toxic effects, which further reduce the implanted cell viability. In this chapter, we will discuss the approach of direct editing of satellite cells in vivo by CRISPR/Cas9 system as a potentially promising alternative method to promote muscle repair in DMD.

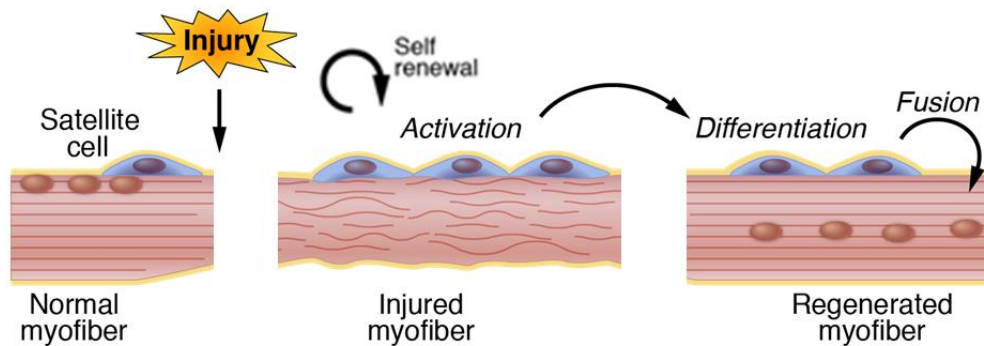


Figure 6.1 Satellite cell-mediated skeletal muscle regeneration

In response to injury, the quiescent satellite cells (left panel) become activated and re-enter the cell cycle (middle panel). The differentiated cells fuse to damaged muscle tissues to generate new myofiber with centralized nuclei (right panel)

6.2 Age-dependent improvement in *mdx-C* mice skeletal muscle

The degree of muscle phenotypic rescue in mosaic mice exceeded the efficiency of gene correction suggests a progressive rescue with age in *mdx-C* mice skeletal muscle. To compare the efficiency of rescue over time, we chose *mdx-C* mice with comparable mosaicism of rescue of approximately 40%. As shown in **Figure 6.2A**, a 3-week *mdx-C* mouse with ~40% HDR-mediated gene correction (termed HDR-40%-3wks) showed occasional dystrophin-negative myofibers amongst a majority of dystrophin-positive fibers. In contrast, no dystrophin-negative fibers were seen in a mouse with comparable gene correction at 9 weeks of age, suggesting progressive rescue with age in skeletal muscle. In *mdx-C* mice with comparable mosaicism, we did not observe a significant difference in dystrophin expression in the heart between 3 and 9 weeks of age (**Figure 6.2B**), suggesting that age-dependent improvement may be restricted to skeletal muscle. This also might reflect the differences in the regeneration ability between heart and skeletal muscle.

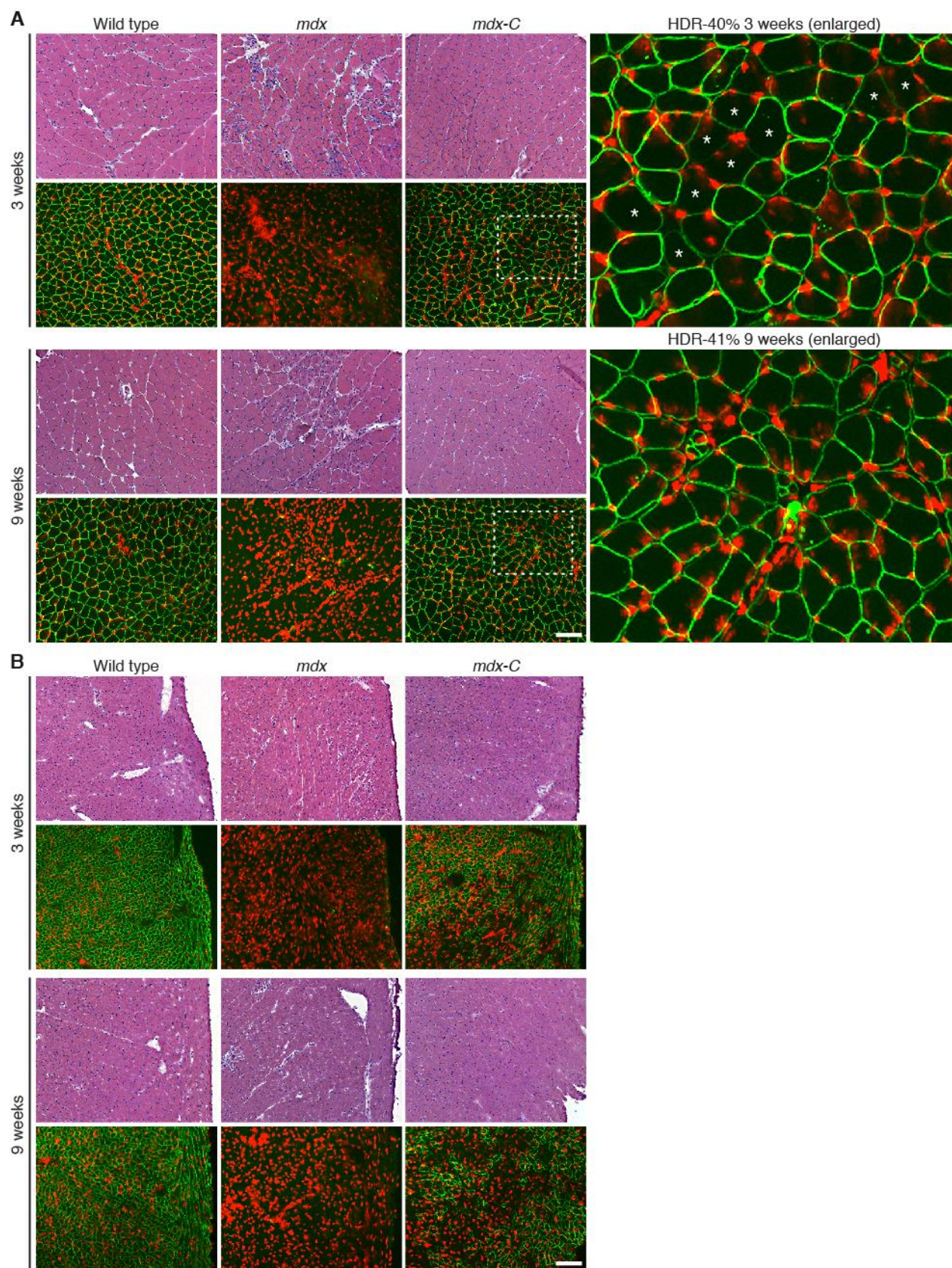


Figure 6.2 Progressive recovery of skeletal muscle not heart following CRISPR/Cas9-mediated genomic editing of *Dmd* allele.

Hematoxylin and eosin (H&E) and dystrophin immunostaining of (A) soleus or (B) heart from 3-week old and 9-week old wild-type, *mdx*, and *mdx-C* mice (3-week-old is HDR-40%-3wk; 9-week old is HDR-41%). Immunofluorescence (green) detects dystrophin. Nuclei are labeled by propidium iodide (red). Magnification of boxed area shows 3-week old (HDR-40%-3wk) and 9-week old (HDR-41%) muscle. At 3-weeks of age many but not all of the myofibers express dystrophin showing partial recovery. White star indicates dystrophin-negative myofibers. By 9-weeks of age, all myofibers in the corrected muscle show dystrophin expression. (B) Although dystrophin expression has been restored in hearts of *mdx-C* mice, no progressive improvement with age is seen from 3-weeks to 9-weeks of age. Scale bar, 100 microns.

Histological analyses of five different muscle types [soleus (hindlimb muscle), gastrocnemius, tibialis, extensor digitorum communis (forelimb muscle), quadriceps and diaphragm (respiratory muscle)] from wild-type mice, *mdx* mice, and HDR-40% *mdx-C* at 3-weeks old are shown in **Figure 6.3**. At 3 weeks of age *mdx* mice, muscle necrosis can be detected in hind limb muscles (soleus, gastrocnemius, tibialis and quadriceps) and respiratory muscle (diaphragm), while forelimb muscle (extensor digitorum communis) has not yet shown histopathologic hallmarks of muscular dystrophy at this age. Despite the presence of a subset of

dystrophin-negative myofibers or partial dystrophin-negative myofibers, HDR-40%-3wk showed absence of the dystrophic muscle phenotype in all muscles.

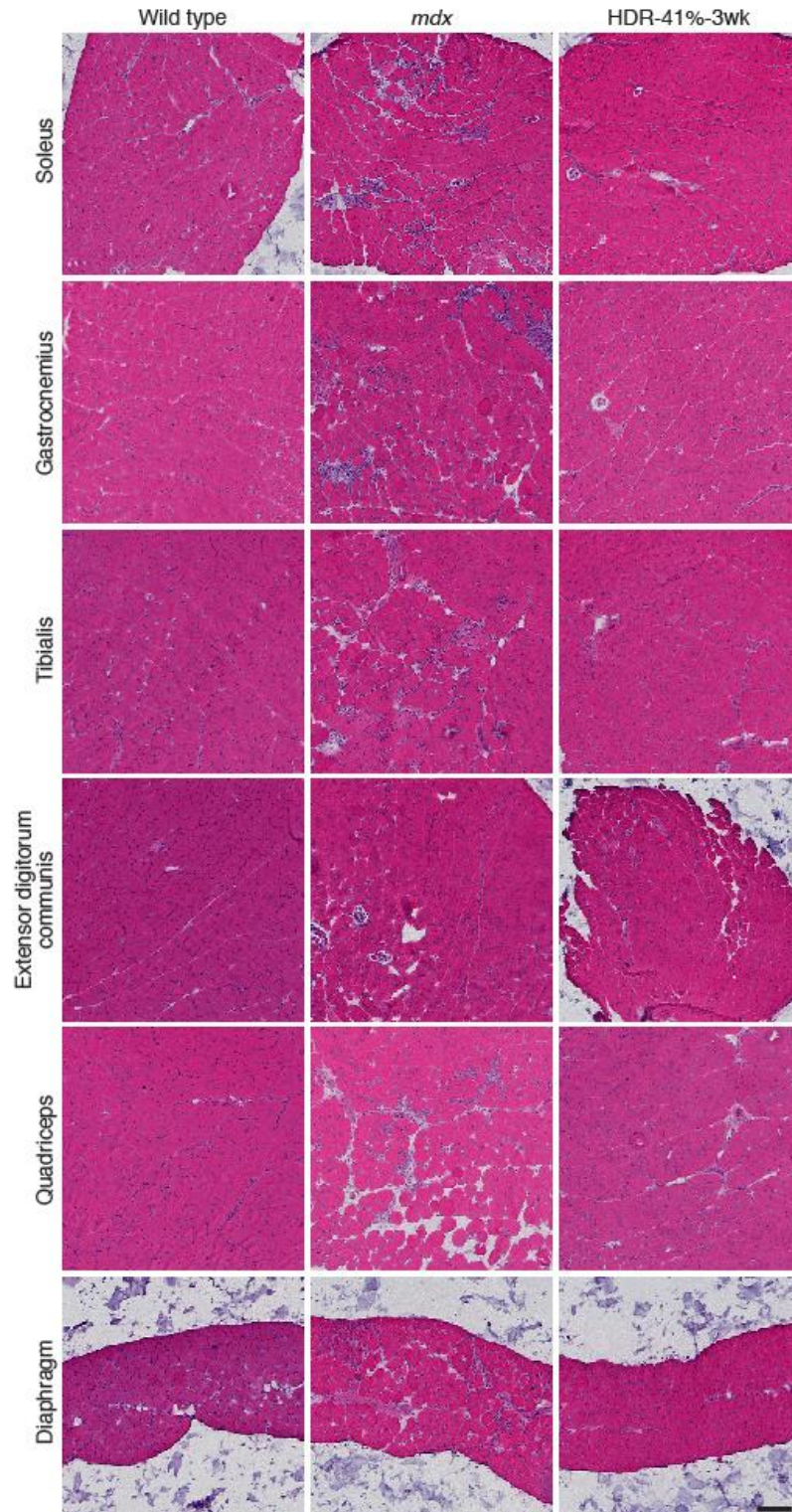


Figure 6.3 Histology of muscles showing decrease in fibrosis and necrosis by CRISPR/Cas9-mediated genomic editing of *Dmd* allele.

Hematoxylin and eosin (H&E) stained transverse cryosections of whole soleus, gastrocnemius, tibialis-anterior, extensor-digitorum-communis, quadriceps, and diaphragm from 3-week old wild-type, *mdx*, HDR-40%-3wk. Scale bar, 125 microns.

6.3 Analysis of satellite cells from *mdx-C* mice

The widespread and progressive rescue of dystrophin expression in skeletal muscle might reflect the multi-nucleated structure of myofibers, such that a subset of nuclei with corrected *Dmd* genes can compensate for nuclei with *Dmd* mutations. Fusion of corrected satellite cells (the stem cell population of skeletal muscle) with dystrophic fibers might also progressively contribute to the regeneration of dystrophic muscle (Yin et al., 2013). To investigate this possibility, we identified satellite cells in muscle sections of *mdx-C* mice by immunostaining with Pax-7, a specific-marker for satellite cells (**Figure 6.4A**). Using laser microdissection, we dissected Pax-7 positive satellite cells and isolated genomic DNA for PCR analysis (**Figure 6.4 B**). Sequencing results of PCR products corresponding to *Dmd* exon 23 from these isolated satellite cells showed the corrected *Dmd* gene (**Figure 6.4C**). These results indicate that CRISPR/Cas9 genomic editing corrected the mutation in satellite cells allowing these muscle stem cells to rescue the dystrophic muscle.

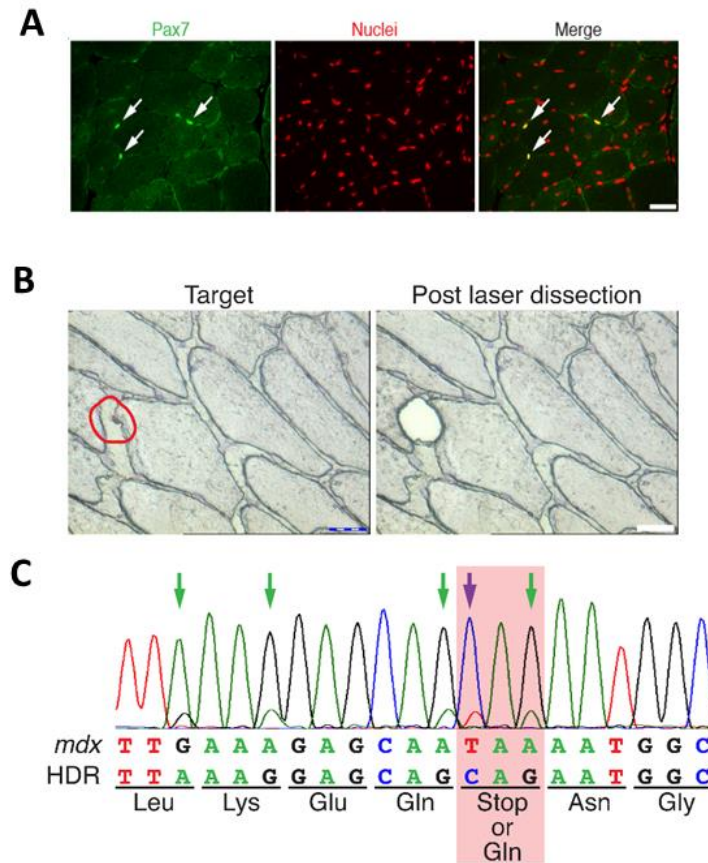


Figure 6. 4 Analysis of satellite cells from *mdx-C* mice.

(A) Cross-section of gastrocnemius from *mdx-C* mouse immunostained for satellite cell-specific marker, Pax7 (left, green) and nuclei (middle, red/propidium iodide). A merged image (right) shows the ‘yellow’ satellite cells located at the edges of the muscle fibers and distinguishes them from “red” myofiber nuclei. White arrows indicate Pax-7 positive satellite cells. Scale bar, 40 microns.

(B) Frozen sections of *mdx-C* gastrocnemius were mounted onto polyethylene membrane frame slides and immunohistochemically stained for Pax-7, a marker for satellite cells. Cross-section of muscle before (left) and after (right) laser dissection shows the precise isolation of satellite cells (brown, in red circle). Scale bar, 25 microns. PCR products corresponding to *Dmd* exon 23 were generated from genomic DNA isolated from satellite

cells of *mdx-C* mice. PCR products were sequenced and show that CRISPR/Cas9-mediated genomic editing corrected a subset of satellite cells in vivo. Purple arrow indicates the corrected allele mediated by HDR. Green arrows indicate the silent mutation sites. The corresponding amino acid residues are shown under the DNA sequence. Red box indicates the corrected site.

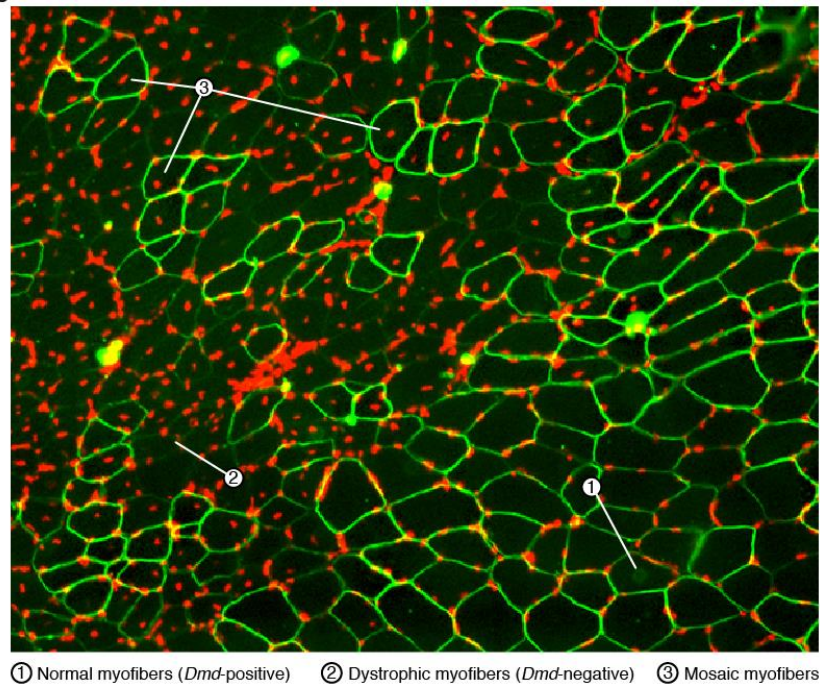


Figure 6. 5 Three types of myofibers in *mdx-C* mice.

Immunostaining of *mdx-C* soleus with anti-dystrophin (green) and propidium iodide (red) highlighting three types of myofibers in the partially corrected *mdx* muscle: 1) normal dystrophin-positive myofibers that originated from CRISPR/Cas9-mediated genome-corrected muscle progenitors; 2) dystrophic dystrophin-negative myofibers that originated from *mdx* mutant progenitors; 3) mosaic dystrophin-positive myofibers with centralized nuclei that formed from fusion of corrected satellite cells with pre-existing dystrophic muscle.

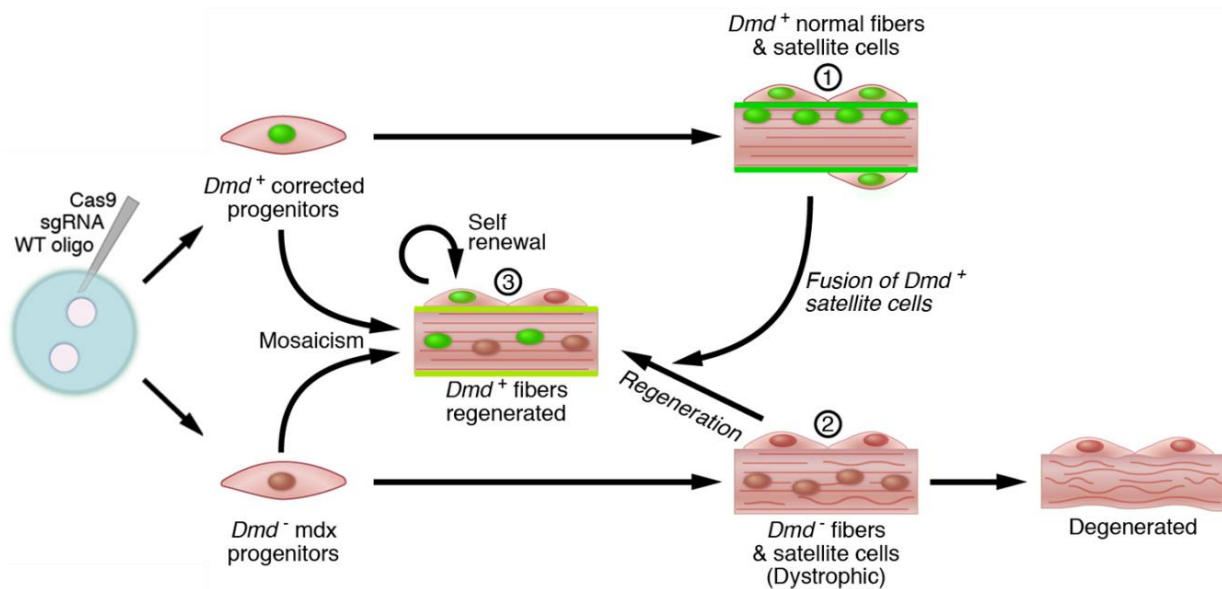


Figure 6.6 A model for rescue of muscular dystrophy by CRISPR/Cas9-mediated genomic correction

6.4 Model to rescue DMD by genomic editing

There are three types of myofibers in *mdx-C* mice: 1) normal dystrophin-positive myofibers (green membrane) and satellite cells originating from corrected progenitors (green nuclei); 2) dystrophic dystrophin-negative myofibers (brown membrane) and satellite cells originating from *mdx* progenitors (brown nuclei); 3) mosaic dystrophin-positive myofibers with centralized nuclei (green and brown nuclei) generated by fusion of corrected and *mdx* progenitors or by fusion of corrected satellite cells with pre-existing dystrophic fibers.

Our results show that CRISPR/Cas9-mediated genomic editing is capable of correcting the primary genetic lesion responsible for muscular dystrophy (DMD) and preventing development of characteristic features of this disease in *mdx* mice. Because genome editing in the germline

produced genetically corrected animals with a wide range of mosaicism (2 to 100%), we were able to compare the percent genomic correction with the extent of rescue of normal muscle structure and function. We observed that only a subset of corrected cells in vivo is sufficient for complete phenotypic rescue. As schematized in **Figure 6.5**, histological analysis of partially corrected *mdx* mice revealed three types of myofibers: 1) Normal dystrophin-positive myofibers; 2) dystrophic dystrophin-negative myofibers; and 3) mosaic dystrophin-positive myofibers containing centralized nuclei, indicative of muscle regeneration. We propose that the latter type of myofiber arises from the recruitment of corrected satellite cells into damaged myofibers, forming mosaic myofibers with centralized nuclei. Efforts to expand satellite cells *ex vivo* as a source of cells for in vivo engraftment have been hindered by the loss of proliferative potential and regenerative capacity of these cells in culture (Montarras et al., 2005). To our knowledge, satellite cell transplantation has not been shown to be successful in the treatment of DMD, at least in part because of the technical challenges associated with transplantation of sufficient numbers of satellite cells into diverse muscles throughout the body to achieve therapeutic benefit. In this regard, Buckingham's group showed that *ex vivo* expansion of wild-type mice satellite cells significantly reduced their in vivo engraftment potential and regenerative capacity. Thus, direct editing of satellite cells in vivo by CRISPR/Cas9 system represents a potentially promising alternative approach to promote muscle repair in DMD.

6. 5 Materials and Methods

6.5.1 Immunostained for satellite cells

Frozen sections from cryoembedments of gastrocnemius were mounted onto polyethylene membrane frame slides (Leica Microsystems PET-Foil 11505151) for same-day set-up of Pax-7 immunohistochemistry. Monoclonal Pax-7 antibody (Developmental Studies Hybridoma Bank) was used as described (Murphy et al., 2011) with modifications to antigen retrieval for working with PET-foil membrane frame slides (Gjerdrum et al., 2001). In brief, gastrocnemius cryosections were air-dried, fixed with 4% paraformaldehyde, Triton-X100 delipidated and incubated in antigen-retrieval buffer (sodium citrate buffer pH 6.0) at 65 °C for 20 hours. Following antigen retrieval, sections were quenched free of endogenous peroxidases with 0.6% hydrogen peroxide, and incubated with mouse IgG blocking reagent (M.O.M. Kit, Vector Laboratories), washed with PBS, incubated with MOM protein concentrate/PBS, and followed by overnight incubation with Pax-7 antibody (2 µg/ml) in MOM protein concentrate/PBS at 4 °C. Sections were washed with PBS and incubated with MOM biotinylated anti-mouse IgG, streptavidin-peroxidase (Vector Laboratories), and color developed with diaminobenzidine chromagen (DAB, Dako). Nuclei were counterstained with nuclease-free Mayer's hematoxylin.

6.5.2 Laser microdissection of satellite cells.

Pax-7 positive satellite cells were microscopically identified and isolated by laser microdissection at 63x objective magnification using a Leica AS-LMD. Sixty to seventy Pax-7 positive satellite cells were isolated for each genotype and pooled into 10 µl of capture buffer (DirectPCR Lysis Reagent, Viagen Biotech Inc.) and stored at -20 °C.

6.5.3 Amplifying the target genomic region by PCR.

The target genomic region was amplified by PCR using primers DMD232_f and DMD232_r (**Table 4.2**), as described before.

Chapter 7 Discussion and future directions

Genomic editing within the germline is not currently feasible in humans. However, genomic editing could, in principle, be envisioned within postnatal cells *in vivo* if certain technical challenges could be overcome.

There is a need for appropriate somatic cell delivery systems capable of directing the components of the CRISPR/Cas9 system to dystrophic muscle or satellite cells *in vivo*. In this regard, the non-pathogenic adeno-associated virus (AAV) delivery system has proven to be safe and effective and has already been advanced in clinical trials for gene therapy (Kotterman and Schaffer, 2014; Nathwani et al., 2011). Moreover, the AAV9 serotype has been shown to provide robust expression in skeletal muscle, heart and brain, the major tissues affected in DMD patients. Other non-viral gene delivery methods, including injection of naked plasmid DNA (Peng et al., 2005), chemically modified mRNA (Kormann et al., 2011; Zangi et al., 2013), and nanoparticles containing nucleic acid (Harris et al., 2010) also warrant consideration.

Another challenge with respect to the feasibility of clinical application of the CRISPR/Cas9 system is the increase in body size between rodents and humans, requiring substantial scale-up. More efficient genome editing in post-natal somatic tissues is also needed for the advancement of the CRISPR/Cas9 system into clinical use.

Although CRISPR/Cas9 can effectively generate NHEJ-mediated indel mutations in somatic cells, HDR-mediated correction is relatively ineffective in postmitotic cells, such as myofibers and cardiomyocytes, because these cells lack the proteins essential for homologous recombination (Hsu et al., 2014). Co-expression of components of the HDR pathway with the CRISPR/Cas9 system might enhance HDR-mediated gene repair.

Finally, safety issues of the CRISPR/Cas9 system, especially for long-term use, need to be evaluated in preclinical studies in large animal models of disease. Despite the challenges listed

above, with rapid technological advances of gene delivery systems and improvements to the CRISPR/Cas9 editing system (Hsu et al., 2014), the approach we describe could ultimately offer therapeutic benefit to DMD and other human genetic diseases in the foreseeable future.

Bibliography

Banks, G.B., and Chamberlain, J.S. (2008). The value of mammalian models for duchenne muscular dystrophy in developing therapeutic strategies. *Current topics in developmental biology* 84, 431-453.

Bulfield, G., Siller, W.G., Wight, P.A., and Moore, K.J. (1984). X chromosome-linked muscular dystrophy (mdx) in the mouse. *Proceedings of the National Academy of Sciences of the United States of America* 81, 1189-1192.

Christian, M., Cermak, T., Doyle, E.L., Schmidt, C., Zhang, F., Hummel, A., Bogdanove, A.J., and Voytas, D.F. (2010). Targeting DNA double-strand breaks with TAL effector nucleases. *Genetics* 186, 757-761.

Cong, L., Ran, F.A., Cox, D., Lin, S., Barretto, R., Habib, N., Hsu, P.D., Wu, X., Jiang, W., Marraffini, L.A., *et al.* (2013). Multiplex genome engineering using CRISPR/Cas systems. *Science* 339, 819-823.

Duan, J., Lu, G., Xie, Z., Lou, M., Luo, J., Guo, L., and Zhang, Y. (2014). Genome-wide identification of CRISPR/Cas9 off-targets in human genome. *Cell Res*, published online (10.1038/cr.2014.1087).

Emery, A.E. (2002). The muscular dystrophies. *Lancet* 359, 687-695.

Fairclough, R.J., Wood, M.J., and Davies, K.E. (2013). Therapy for Duchenne muscular dystrophy: renewed optimism from genetic approaches. *Nature reviews Genetics* 14, 373-378.

Fu, Y., Foden, J.A., Khayter, C., Maeder, M.L., Reyon, D., Joung, J.K., and Sander, J.D. (2013). High-frequency off-target mutagenesis induced by CRISPR-Cas nucleases in human cells. *Nature biotechnology* 31, 822-826.

Fu, Y., Sander, J.D., Reyon, D., Cascio, V.M., and Joung, J.K. (2014). Improving CRISPR-Cas nuclease specificity using truncated guide RNAs. *Nature biotechnology* 32, 279-284.

Fujii, W., Kawasaki, K., Sugiura, K., and Naito, K. (2013). Efficient generation of large-scale genome-modified mice using gRNA and CAS9 endonuclease. *Nucleic acids research* 41, e187.

Gjerdrum, L.M., Lielpetere, I., Rasmussen, L.M., Bendix, K., and Hamilton-Dutoit, S. (2001). Laser-assisted microdissection of membrane-mounted paraffin sections for polymerase chain reaction analysis: identification of cell populations using immunohistochemistry and in situ hybridization. *J Mol Diagn* 3, 105-110.

Grounds, M.D., Radley, H.G., Lynch, G.S., Nagaraju, K., and De Luca, A. (2008). Towards developing standard operating procedures for pre-clinical testing in the mdx mouse model of Duchenne muscular dystrophy. *Neurobiology of disease* 31, 1-19.

Guan, C., Ye, C., Yang, X., and Gao, J. (2010). A review of current large-scale mouse knockout efforts. *Genesis* 48, 73-85.

Hall, B., Limaye, A., and Kulkarni, A.B. (2009). Overview: generation of gene knockout mice. *Current protocols in cell biology / editorial board, Juan S Bonifacino [et al] Chapter 19, Unit 19* 12 19 12 11-17.

Harris, T.J., Green, J.J., Fung, P.W., Langer, R., Anderson, D.G., and Bhatia, S.N. (2010). Tissue-specific gene delivery via nanoparticle coating. *Biomaterials* 31, 998-1006.

Hoffman, E.P., Brown, R.H., Jr., and Kunkel, L.M. (1987). Dystrophin: the protein product of the Duchenne muscular dystrophy locus. *Cell* 51, 919-928.

Hsu, P.D., Lander, E.S., and Zhang, F. (2014). Development and Applications of CRISPR-Cas9 for Genome Engineering. *Cell* 157, 1262-1278.

Hsu, P.D., Scott, D.A., Weinstein, J.A., Ran, F.A., Konermann, S., Agarwala, V., Li, Y., Fine, E.J., Wu, X., Shalem, O., *et al.* (2013). DNA targeting specificity of RNA-guided Cas9 nucleases. *Nature biotechnology* 31, 827-832.

Jinek, M., Chylinski, K., Fonfara, I., Hauer, M., Doudna, J.A., and Charpentier, E. (2012). A programmable dual-RNA-guided DNA endonuclease in adaptive bacterial immunity. *Science* 337, 816-821.

Kim, J.S., Lee, H.J., and Carroll, D. (2010). Genome editing with modularly assembled zinc-finger nucleases. *Nature methods* 7, 91; author reply 91-92.

Kim, Y.G., Cha, J., and Chandrasegaran, S. (1996). Hybrid restriction enzymes: zinc finger fusions to Fok I cleavage domain. *Proceedings of the National Academy of Sciences of the United States of America* 93, 1156-1160.

Kodippili, K., Vince, L., Shin, J.H., Yue, Y., Morris, G.E., McIntosh, M.A., and Duan, D. (2014). Characterization of 65 epitope-specific dystrophin monoclonal antibodies in canine and murine models of duchenne muscular dystrophy by immunostaining and western blot. *PloS one* 9, e88280.

Kormann, M.S., Hasenpusch, G., Aneja, M.K., Nica, G., Flemmer, A.W., Herber-Jonat, S., Huppmann, M., Mays, L.E., Illenyi, M., Schams, A., *et al.* (2011). Expression of therapeutic proteins after delivery of chemically modified mRNA in mice. *Nature biotechnology* 29, 154-157.

Kotterman, M.A., and Schaffer, D.V. (2014). Engineering adeno-associated viruses for clinical gene therapy. *Nature reviews Genetics* 15, 445-451.

Kuscu, C., Arslan, S., Singh, R., Thorpe, J., and Adli, M. (2014). Genome-wide analysis reveals characteristics of off-target sites bound by the Cas9 endonuclease. *Nature biotechnology* 32, 677-683.

Mali, P., Aach, J., Stranges, P.B., Esvelt, K.M., Moosburner, M., Kosuri, S., Yang, L., and Church, G.M. (2013a). CAS9 transcriptional activators for target specificity screening and paired nickases for cooperative genome engineering. *Nature biotechnology* 31, 833-838.

Mali, P., Esvelt, K.M., and Church, G.M. (2013b). Cas9 as a versatile tool for engineering biology. *Nature methods* 10, 957-963.

Mali, P., Yang, L., Esvelt, K.M., Aach, J., Guell, M., DiCarlo, J.E., Norville, J.E., and Church, G.M. (2013c). RNA-guided human genome engineering via Cas9. *Science* 339, 823-826.

Mauro, A. (1961). Satellite cell of skeletal muscle fibers. *The Journal of biophysical and biochemical cytology* 9, 493-495.

Monaco, A.P., Neve, R.L., Colletti-Feener, C., Bertelson, C.J., Kurnit, D.M., and Kunkel, L.M. (1986). Isolation of candidate cDNAs for portions of the Duchenne muscular dystrophy gene. *Nature* 323, 646-650.

Montarras, D., Morgan, J., Collins, C., Relaix, F., Zaffran, S., Cumano, A., Partridge, T., and Buckingham, M. (2005). Direct isolation of satellite cells for skeletal muscle regeneration. *Science* *309*, 2064-2067.

Murphy, M.M., Lawson, J.A., Mathew, S.J., Hutcheson, D.A., and Kardon, G. (2011). Satellite cells, connective tissue fibroblasts and their interactions are crucial for muscle regeneration. *Development* *138*, 3625-3637.

Nathwani, A.C., Rosales, C., McIntosh, J., Rastegarlar, G., Nathwani, D., Raj, D., Nawathe, S., Waddington, S.N., Bronson, R., Jackson, S., *et al.* (2011). Long-term safety and efficacy following systemic administration of a self-complementary AAV vector encoding human FIX pseudotyped with serotype 5 and 8 capsid proteins. *Molecular therapy : the journal of the American Society of Gene Therapy* *19*, 876-885.

Nicholson, L.V., Davison, K., Falkous, G., Harwood, C., O'Donnell, E., Slater, C.R., and Harris, J.B. (1989). Dystrophin in skeletal muscle. I. Western blot analysis using a monoclonal antibody. *J Neurol Sci* *94*, 125-136.

Pattanayak, V., Lin, S., Guilinger, J.P., Ma, E., Doudna, J.A., and Liu, D.R. (2013). High-throughput profiling of off-target DNA cleavage reveals RNA-programmed Cas9 nuclease specificity. *Nature biotechnology* *31*, 839-843.

Paulk, N.K., Wursthorn, K., Wang, Z., Finegold, M.J., Kay, M.A., and Grompe, M. (2010). Adeno-associated virus gene repair corrects a mouse model of hereditary tyrosinemia in vivo. *Hepatology* *51*, 1200-1208.

Peng, B., Zhao, Y., Lu, H., Pang, W., and Xu, Y. (2005). In vivo plasmid DNA electroporation resulted in transfection of satellite cells and lasting transgene expression in regenerated muscle fibers. *Biochem Biophys Res Commun* 338, 1490-1498.

Pigozzo, S.R., Da Re, L., Romualdi, C., Mazzara, P.G., Galletta, E., Fletcher, S., Wilton, S.D., and Vitiello, L. (2013). Revertant fibers in the mdx murine model of Duchenne muscular dystrophy: an age- and muscle-related reappraisal. *PloS one* 8, e72147.

Posfai, G., Kolisnychenko, V., Berezki, Z., and Blattner, F.R. (1999). Markerless gene replacement in *Escherichia coli* stimulated by a double-strand break in the chromosome. *Nucleic acids research* 27, 4409-4415.

Ran, F.A., Hsu, P.D., Lin, C.Y., Gootenberg, J.S., Konermann, S., Trevino, A.E., Scott, D.A., Inoue, A., Matoba, S., Zhang, Y., *et al.* (2013). Double nicking by RNA-guided CRISPR Cas9 for enhanced genome editing specificity. *Cell* 154, 1380-1389.

Sadoulet-Puccio, H.M., and Kunkel, L.M. (1996). Dystrophin and its isoforms. *Brain pathology* 6, 25-35.

Schwank, G., Koo, B.K., Sasselli, V., Dekkers, J.F., Heo, I., Demircan, T., Sasaki, N., Boymans, S., Cuppen, E., van der Ent, C.K., *et al.* (2013). Functional repair of CFTR by CRISPR/Cas9 in intestinal stem cell organoids of cystic fibrosis patients. *Cell stem cell* 13, 653-658.

Shen, B., Zhang, W., Zhang, J., Zhou, J., Wang, J., Chen, L., Wang, L., Hodgkins, A., Iyer, V., Huang, X., *et al.* (2014). Efficient genome modification by CRISPR-Cas9 nickase with minimal off-target effects. *Nature methods* 11, 399-402.

van Deutekom, J.C., and van Ommen, G.J. (2003). Advances in Duchenne muscular dystrophy gene therapy. *Nature reviews Genetics* 4, 774-783.

Wang, H., Yang, H., Shivalila, C.S., Dawlaty, M.M., Cheng, A.W., Zhang, F., and Jaenisch, R. (2013). One-step generation of mice carrying mutations in multiple genes by CRISPR/Cas-mediated genome engineering. *Cell* 153, 910-918.

Wei, C., Liu, J., Yu, Z., Zhang, B., Gao, G., and Jiao, R. (2013). TALEN or Cas9 - rapid, efficient and specific choices for genome modifications. *J Genet Genomics* 40, 281-289.

Wood, M.J. (2013). To skip or not to skip: that is the question for duchenne muscular dystrophy. *Molecular therapy : the journal of the American Society of Gene Therapy* 21, 2131-2132.

Worton, R.G., and Thompson, M.W. (1988). Genetics of Duchenne muscular dystrophy. *Annu Rev Genet* 22, 601-629.

Wu, X., Scott, D.A., Kriz, A.J., Chiu, A.C., Hsu, P.D., Dadon, D.B., Cheng, A.W., Trevino, A.E., Konermann, S., Chen, S., *et al.* (2014). Genome-wide binding of the CRISPR endonuclease Cas9 in mammalian cells. *Nature biotechnology* 32, 670-676.

Wu, Y., Liang, D., Wang, Y., Bai, M., Tang, W., Bao, S., Yan, Z., Li, D., and Li, J. (2013). Correction of a genetic disease in mouse via use of CRISPR-Cas9. *Cell stem cell* 13, 659-662.

Xue, W., Chen, S., Yin, H., Tammela, T., Papagiannakopoulos, T., Joshi, N.S., Cai, W., Yang, G., Bronson, R., Crowley, D.G., *et al.* (2014). CRISPR-mediated direct mutation of cancer genes in the mouse liver. *Nature* 514, 380-384.

Yang, H., Wang, H., Shivalila, C.S., Cheng, A.W., Shi, L., and Jaenisch, R. (2013a). One-step generation of mice carrying reporter and conditional alleles by CRISPR/Cas-mediated genome engineering. *Cell* 154, 1370-1379.

Yang, L., Guell, M., Byrne, S., Yang, J.L., De Los Angeles, A., Mali, P., Aach, J., Kim-Kiselak, C., Briggs, A.W., Rios, X., *et al.* (2013b). Optimization of scarless human stem cell genome editing. *Nucleic acids research* 41, 9049-9061.

Yen, S.T., Zhang, M., Deng, J.M., Usman, S.J., Smith, C.N., Parker-Thornburg, J., Swinton, P.G., Martin, J.F., and Behringer, R.R. (2014). Somatic mosaicism and allele complexity induced by CRISPR/Cas9 RNA injections in mouse zygotes. *Dev Biol*, published online (10.1016/j.ydbio.2014.1006.1017).

Yin, H., Price, F., and Rudnicki, M.A. (2013). Satellite cells and the muscle stem cell niche. *Physiol Rev* 93, 23-67.

Yin, H., Xue, W., Chen, S., Bogorad, R.L., Benedetti, E., Grompe, M., Koteliansky, V., Sharp, P.A., Jacks, T., and Anderson, D.G. (2014). Genome editing with Cas9 in adult mice corrects a disease mutation and phenotype. *Nature biotechnology* 32, 551-553.

Yoshimi, K., Kaneko, T., Voigt, B., and Mashimo, T. (2014). Allele-specific genome editing and correction of disease-associated phenotypes in rats using the CRISPR-Cas platform. *Nature communications* 5, 4240.

Zangi, L., Lui, K.O., von Gise, A., Ma, Q., Ebina, W., Ptaszek, L.M., Spater, D., Xu, H., Tabebordbar, M., Gorbатов, R., *et al.* (2013). Modified mRNA directs the fate of heart progenitor

cells and induces vascular regeneration after myocardial infarction. *Nature biotechnology* 31, 898-907.